



## Research papers

# Temperature buffering by groundwater in ecologically valuable lowland streams under current and future climate conditions



Vince P. Kaandorp<sup>a,b,\*</sup>, Pieter J. Doornenbal<sup>a</sup>, Henk Kooi<sup>a</sup>, Hans Peter Broers<sup>c</sup>, Perry G.B. de Louw<sup>a,d</sup>

<sup>a</sup> Department of Subsurface and Groundwater Systems, Deltares, Utrecht, the Netherlands

<sup>b</sup> Department of Earth Sciences, Utrecht University, Utrecht, the Netherlands

<sup>c</sup> TNO Geological Survey of the Netherlands, Utrecht, the Netherlands

<sup>d</sup> Soil Physics and Land Management, Wageningen University, Wageningen, the Netherlands

## ARTICLE INFO

## Article history:

Received 19 November 2018

Revised 11 March 2019

Accepted 12 March 2019

Available online 14 March 2019

## Keywords:

Stream temperature

Groundwater-surface water interaction

Distributed temperature sensing

Stream temperature model

Radon-222

Climate change

## ABSTRACT

Groundwater seepage influences the temperature of streams and rivers by providing a relatively cool input in summer and warm input in winter. Because of this, groundwater seepage can be a determining factor in the provision of suitable water temperatures for aquatic biota. Climate warming affects stream and groundwater temperatures, and changes the thermal characteristics of streams leading to the potential disappearance of habitats. In this study the importance of groundwater for the temperature of two Dutch lowland streams and its possible role in mitigating the effects of climate change was determined by combining field measurements and a modelling experiment. Stream temperature measurements using fibre optic cables (FO-DTS) and sampling of <sup>222</sup>Rn were done to map localized groundwater inflow. Several springs and seepage 'hot-spots' were located which buffered the water temperature in summer and winter. A stream temperature model was constructed and calibrated using the FO-DTS-measurements to quantify the energy fluxes acting on stream water. This way, the contribution to the stream thermal budget of direct solar radiation, air temperature and seepage were separated. The model was then used to simulate the effects of changes in shading, groundwater seepage and climate. Shading was shown to be an important control on summer temperature maxima. Groundwater seepage seemed to buffer the effect of climate warming, potentially making groundwater dominated streams more climate robust. Protecting groundwater resources in a changing climate is important for the survival of aquatic species in groundwater-fed systems, as groundwater seepage both sustains flow and buffers temperature extremes.

© 2019 The Authors. Published by Elsevier B.V. This is an open access article under the CC BY-NC-ND license (<http://creativecommons.org/licenses/by-nc-nd/4.0/>).

## 1. Introduction

Stream water temperature is an important factor influencing aquatic ecosystems as it affects species distribution, growth, metabolism and reproduction (Vannote and Sweeney, 1980), as well as oxygen concentrations, biological production and decomposition (Bowes et al., 2016; Haidekker and Hering, 2008; Hawkins et al., 1997; Ormerod, 2009; Rasmussen et al., 2011; Ward and Stanford, 1982; Ylla et al., 2014). Consequently, changes in stream temperature can act as a stressor on aquatic species (e.g. Piggott et al., 2015; Poole and Berman, 2001; Schülting et al., 2016). It is therefore not surprising that much research has been done on the effect of climate warming on stream temperature and aquatic

species (e.g. Eaton and Scheller, 1996; Guse et al., 2015; Isaak et al., 2018, 2015; Moss et al., 2003; Null et al., 2012). It is expected that in a warmer global climate the average and peak temperature of stream water will increase (Van Vliet et al., 2013; Watts et al., 2015; Webb and Nobilis, 2007).

Many studies on stream temperature have focused on the effect of air temperature, radiation and shading (e.g. Garner et al., 2017; Hannah et al., 2008; Macdonald et al., 2014; Westhoff et al., 2011). Due to these studies, it is now widely recognized that riparian shade reduces maximum stream temperatures in summer by blocking part of the incoming solar radiation (Dugdale et al., 2018; Sweeney and Newbold, 2014; Thomas et al., 2015), and therefore, that management practices like planting vegetation along streams can potentially mitigate the effect of climate warming (Kristensen et al., 2015; Nash et al., 2018; Thomas et al., 2015).

Groundwater temperature is influenced by the temperature of the infiltrating water and by the conduction of heat from the

\* Corresponding author at: Department of Subsurface and Groundwater Systems, Deltares, Utrecht, the Netherlands.

E-mail address: [Vince.Kaandorp@deltares.nl](mailto:Vince.Kaandorp@deltares.nl) (V.P. Kaandorp).

surface. The impact of diurnal to seasonal variations of surface temperature dampens with depth. Downward from the surface, groundwater temperature, therefore, tends to approach the yearly average ground surface temperature (e.g. Bense and Kooi, 2004; de Louw et al., 2010; Vandenbohede et al., 2014). In areas with strong upward seepage, this moderate groundwater temperature is carried into streams. Therefore, groundwater seepage into streams is known to moderate summer and winter stream temperatures, and to create so called local *thermal refugia* (e.g. Hayashi and Rosenberry, 2002; Kaandorp et al., 2018b; Power et al., 1999) and *climate refugia* (e.g. Briggs et al., 2018b; Isaak et al., 2015; Meisner et al., 1988) for aquatic biota. Although the role of groundwater on stream temperatures is conceptually understood, its effect is often neglected or highly simplified in studies on stream temperature and almost never considered in stream temperature management. Therefore, the influence of groundwater on stream temperature and the subsequent response of aquatic ecology still requires more research.

The objective of this study is to determine the influence of groundwater on the temperature of two Dutch lowland streams and to get insight into its possible role in mitigating the effects of climate change. For this, both field measurements and a modelling experiment are done. Research questions are: a) what is the spatial variability of groundwater seepage to the streams, b) what is the spatial and temporal effect of groundwater seepage on stream temperature, c) how does the effect of groundwater inflow on stream temperature compare to the effect of air temperature and radiation (including shading), and d) what is the effect of groundwater on stream temperature in a warming climate?

We combine different field techniques such as Fibre Optic Distributed Temperature Sensing (FO-DTS) and measurements of the isotope  $^{222}\text{Rn}$  to detect diffuse and localized groundwater inputs to the two Dutch lowland streams. FO-DTS is used to make high resolution temperature measurements, both in time and space (Selker et al., 2006). Compared to surface water, the temperature of groundwater is relatively constant throughout the year and as such lateral changes in stream water temperature can be used to locate groundwater seepage zones in specific moments in time (Briggs et al., 2012; Krause et al., 2012; Matheswaran et al., 2014b; Poulsen et al., 2015; Rosenberry et al., 2016; Sebok et al., 2013; Vandenbohede et al., 2014; Westhoff et al., 2007). The presence of the isotope  $^{222}\text{Rn}$  in surface water also indicates recent seepage of groundwater, as it is rapidly removed in surface waters by radioactive decay and degassing. In addition to this field data, we construct a stream temperature model, which includes the effects of air temperature, radiation, shading and groundwater seepage. The model is used to analyze the behavior of the different processes affecting stream temperature. By applying different scenarios we derive the effect of climate change on stream thermal habitats and the mitigating effects of groundwater seepage.

## 2. Study area and methods

### 2.1. Study area

Field measurements were done in two lowland streams in the east of the Netherlands: the Springendalse Beek and the Elsbeek (Fig. 1). With catchments sizes of 4 km<sup>2</sup> and 11 km<sup>2</sup> respectively, these streams discharge to the Dinkel river. The area has a temperate marine climate with a mean annual air temperature of 9.6 °C and mean annual precipitation and evaporation of 850 and 560 mm per year respectively. The average discharge is 0.043 m<sup>3</sup> s<sup>-1</sup> for the Springendalse Beek and 0.104 m<sup>3</sup> s<sup>-1</sup> for the Elsbeek. The subsurface of the catchments consists of shallow aquifers (1–20 m thick) on top of clayey moraines. The streambed of

the streams consists of sand with occasionally some gravel. Details on the study catchments were described by Kaandorp et al. (2018b). A concise description of the studied stream stretches is given here.

The upstream catchment of the Springendalse Beek contains a few distinct spring areas and consists mainly of forest with some agricultural fields. The studied stream stretch extends 1500 m downstream from the stream origin (Fig. 1a). The upstream part has a relatively stable discharge, a stream width between 0.5 and 1.0 m and a water depth of a few centimetres. A small spring, a tributary, two seepage ponds and tributaries from a swamp discharge into the stream (Fig. 1a). The downstream part has a width of 1.0–1.5 m and a water depth of around 10 cm.

The Elsbeek predominantly consists of agricultural areas. The measured stream stretch extends from approximately 5000 to 6500 m downstream from the stream origin (Fig. 1b). The most upstream 200 m of the study stretch is straightened, flows through an agricultural area and has a width of about 1 m and a water depth of around 5 cm. Here the outflow of an agricultural ditch, which dries up during summer, joins the stream. This is followed by a stream stretch with a riparian forest and a pool-riffle sequence with pools up to 1 m deep and a width varying between 0.5 and 1.5 m. A stretch with a length of 150 m in the central part is again straightened and flows through an agricultural area with a width of around 1 m and a water depth of about 30 cm. After this an agricultural ditch joins the stream. The most downstream part of the studied stream stretch flows again through a forest, is shallow (~3–10 cm) and has a width varying between 0.5 and 2.0 m. This part of the stream is deeply incised (1.0–1.5 m) into the landscape.

### 2.2. FO-DTS set-up

Stream temperatures were measured using an Oryx DTS (Sensornet USA) unit and CTC LSZH fibre-optic cables (TKF Connectivity Solutions, Netherlands). A cable with a length of 1300 m was positioned in the study stretch of the Springendalse Beek, from 200 m downstream from the stream origin ( $x=200$ ) to the end of the studied stream stretch ( $x=1500$ ) (Fig. 1). At  $x=305$  and  $x=435$ , the cable was looped back and forth through a small spring directly next to the stream ( $x=305$ ), and in a side branch of the stream ( $x=435$ ), respectively (Fig. 1a). Approximately 1500 m of fibre optic cable was installed in the Elsbeek, covering the two forested stream stretches and two open areas (Fig. 1b). In both streams, the cable was installed on the streambed, and fixed using U shaped metal pegs. A double ended configuration was used with two calibration baths next to the Oryx unit and a splice at the end of the fibre optic cable. By using the double ended setup corrections for splices and light attenuation in the fibre optic cable can be made (Hausner et al., 2011; Van De Giesen et al., 2012). For calibration, a coil of cable was placed in each isolated calibration bath which was equipped with a PT-100 temperature sensor and connected with the Oryx unit. Measurements were done for the whole months of August 2016 and January 2017 to capture both summer and winter temperature patterns. Each DTS measurement was done with a spatial resolution of 1.0 m and consisted of sequential measuring of 5 min through 2 channels, which were repeated either every half an hour (summer) or every hour (winter).

Because the DTS cable was placed on the streambed the measurements represent the temperature at the bottom of the stream, unless it was buried by sediments. Sediment was removed from the DTS cable several times, but it could not be prevented that during part of the measurement period some parts of the cable were buried by sediment. In the streambed the temperature variation present in the stream is attenuated with depth, and as such sedimentation leads to a temperature signal comparable to that of

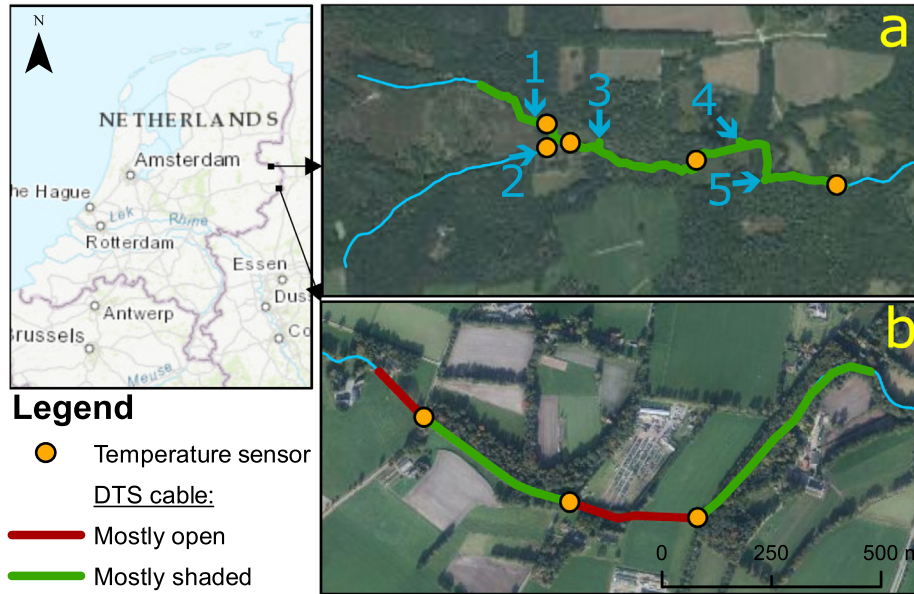


**Fig. 1.** Location of the fibre optic cables and temperature sensors in the Springendalse Beek (a) and Elsbeek (b). The numbered arrows 1 to 5 in panel a indicate inflow from a spring (1), tributary (2), small and large groundwater-fed ponds (3 and 4) and tributaries swamp (5).

groundwater seepage, such as a decrease in the standard deviation (SD) of the temperature (Sebok et al., 2015).

The DTS temperature measurements were calibrated using dispersion, slope and offset corrections which followed from the calibration baths. Further corrections for offsets were applied using Onset 12-Bit temperature smart sensors (S-TMB-M006) with HOBO data loggers (H21-001) which were installed just above the stream bed at 5 locations in the Springendalse Beek and 3 locations in the Elsbeek (Fig. 1). Comparison of the separate temperature sensors and the corrected DTS temperature measurements showed that stream temperatures could be measured with an accuracy of 0.19 °C on average. Temperatures were logged every 15 min and some of the loggers were supplied with an extra sensor to measure air temperature. Additional weather data was collected from nearby meteorological station Twenthe of the Royal Netherlands Meteorological Institute (KNMI).

### 2.3. Radon measurements

$^{222}\text{Rn}$ , an isotope released to the groundwater from aquifer material, was used as a tracer for groundwater in along-stream profiling (Cartwright et al., 2014; Cook et al., 2006; Genereux and Hemond, 1990). Samples were taken and measured immediately in the field using an Electronic Radon Detector (RAD7, DurrIDGE). High radon values in streams were expected to be found only near locations with groundwater seepage because it rapidly decays (half-life of 3.8 days) and is released to the atmosphere due to degassing.

### 2.4. Stream temperature model

A stream temperature model (STM-GW) was built in Python using the xarray-simlab model framework (Bovy and McBain, 2017). The model is largely based on the model descriptions of Boyd and Kasper (2003) and Westhoff et al. (2007) and additionally simulates the interaction with groundwater in more detail (Fig. 2). In the model, all water fluxes ( $Q$ ) are considered constant in time and only increase in the downstream direction due to groundwater and lateral inflow. The stream stretch is discretized into a 1D cell-centred grid and to prevent numerical diffusion a Courant number

of 1 is used. For this, the size of the stream cells fluctuates spatially with the flow velocity, which depends on the discharge, depth and stream width:

$$C = \frac{v_i * \Delta t}{\Delta x_i} = 1 \quad (1)$$

$$v_i = \frac{Q_i}{A_i} \quad (2)$$

$$\Delta x_i = \frac{Q_i}{A_i} \Delta t \quad (3)$$

where  $C$  is the Courant number [-],  $v_i$  is the flow velocity in cell  $i$  [ $\text{m s}^{-1}$ ],  $\Delta t$  the time step [s] and  $\Delta x_i$  the cell size [m].  $Q_i$  is the discharge at the downstream end of the cell [ $\text{m}^3 \text{s}^{-1}$ ] and  $A_i$  is the cross-sectional area [ $\text{m}^2$ ] of the stream. The temperature in each cell is then calculated using:

$$T_i^{j+1} = \frac{T_i^j V_i + T_{GW}^j V_{GW} + T_{agri}^j V_{agri} + T_{pond}^j V_{pond}}{V_i + V_{GW} + V_{agri} + V_{pond}} - \frac{v \Delta t}{\left(\frac{\Delta x_i + \Delta x_{i-1}}{2}\right)} \left(T_i^j - T_{i-1}^j\right) + \frac{R_i^j \Delta t}{A_i} \quad (4)$$

where  $T_i^{j+1}$  is the water temperature in the stream [°C] at grid cell  $i$  at the new time level  $j + 1$ ,  $j$  denotes the old time level and  $i - 1$  the grid cell upstream from cell  $i$ . The first term is the mixing term, the second term is the advection term and the third term is the temperature change due to the source/sink term. In a stream with no advection or energy source/sink but with only mixing from inflows (Fig. 2), the temperature is given by only by the mixing term:

$$T_i^{j+1} = \frac{T_i^j V_i + T_{GW}^j V_{GW} + T_{agri}^j V_{agri} + T_{pond}^j V_{pond}}{V_i + V_{GW} + V_{agri} + V_{pond}} \quad (5)$$

where  $T_i^j$  is the temperature [°C] and  $V_i$  the volume [ $\text{m}^3$ ] of cell  $i$  at time  $j$ .  $V_{GW}$ ,  $V_{agri}$  and  $V_{pond}$  are the volumes [ $\text{m}^3$ ] of inflow per time step from groundwater, tributaries and seepage ponds respectively, and  $T_{GW}^j$ ,  $T_{agri}^j$  and  $T_{pond}^j$  are their temperatures at time  $j$ . With only

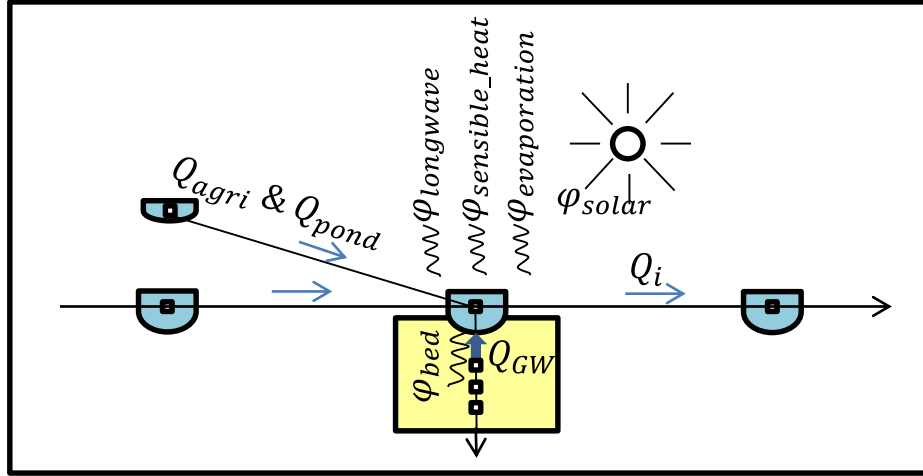


**Fig. 2.** Conceptualization of the STM-GW model. A stream cell can receive water from an upstream cell and from lateral inflow such as from tile drainage or seepage ponds. Each cell exchanges energy with the atmosphere by solar and longwave radiation, and latent and sensible heat flow. Each stream cell is connected to cells that represent the streambed to represent groundwater inflow and conductive heat exchange with the streambed.

advection, the stream temperature is given by the advection term (Eq. (4)):

$$T_i^{j+1} = T_i^j - \frac{v\Delta t}{\left(\frac{\Delta x_i + \Delta x_{i-1}}{2}\right)} (T_i^j - T_{i-1}^j) \quad (6)$$

where  $\frac{\Delta x_i + \Delta x_{i-1}}{2}$  is the average cell size between grid cell  $i$  and upstream cell  $i - 1$  [m], which is needed because of the increase in cell size in the downstream direction. For simplicity dispersion is assumed to be negligible (e.g. Irvine et al., 2017; Rau et al., 2012). The temperature development of a stagnant body of water without inflow is determined by the source/sink term  $R$  (Eq. (4)), which includes all the energy fluxes that act on the water body:

$$R_i^j = \frac{B_i \varphi_{total}^j}{\rho_w c_w} \quad (7)$$

$$T_i^{j+1} = T_i^j + \frac{R_i^j \Delta t}{A_i} \quad (8)$$

where  $B_i$  is the stream width [m] of cell  $i$ ,  $c_w$  and  $\rho_w$  are the specific heat and density of the water and  $\varphi_{total}$  is the sum of all the energy fluxes per unit horizontal area [ $W m^{-2}$ ].

$\varphi_{total}$  is calculated for each cell for every time step and includes the various energy fluxes that influence stream temperature: solar radiation ( $\varphi_{solar}$ ), longwave radiation ( $\varphi_{longwave}$ ), latent heat flow ( $\varphi_{evaporation}$ ), sensible heat flow ( $\varphi_{sensible\_heat}$ ) and streambed conduction ( $\varphi_{bed}$ ) (Fig. 2):

$$\varphi_{total} = \varphi_{solar} + \varphi_{longwave} + \varphi_{evaporation} + \varphi_{sensible\_heat} + \varphi_{bed} \quad (9)$$

Solar radiation ( $\varphi_{solar}$ ) [ $W m^{-2}$ ] consists of both direct radiation and diffuse radiation which is described by fraction  $D_{diffuse}$  of the incoming radiation ( $\varphi_{inRad}$ ). A fraction  $D_f$  of the solar radiation penetrates the water and heats the streambed instead. Surface reflection coefficient  $R_{SS}$  corrects for reflection of solar radiation on the water surface and is based on the solar angle for direct radiation and is equal to 0.09 for diffuse radiation (Boyd and Kasper, 2003). Direct radiation is additionally corrected for shadow effects by shading factor  $C_s$  (Westhoff et al., 2007).

$$\varphi_{solar} = (1 - D_f)(\varphi_{direct} + \varphi_{diffuse}) \quad (10)$$

$$\varphi_{direct} = C_s(1 - D_{diffuse})(1 - R_{SS})\varphi_{inRad} \quad (11)$$

$$\varphi_{diffuse} = D_{diffuse}(1 - R_{SS})\varphi_{inRad} \quad (12)$$

Longwave radiation ( $\varphi_{longwave}$ ) [ $W m^{-2}$ ] is the sum of the longwave radiation from clouds (atmospheric), back radiation from the water column and radiation emitted by the land cover (e.g. vegetation) (Boyd and Kasper, 2003):

$$\varphi_{longwave} = \varphi_{atmospheric} + \varphi_{back\_radiation} + \varphi_{land\_cover} \quad (13)$$

$$\varphi_{atmospheric} = 0.96\epsilon_{atm}\theta_{VTS}\sigma_{sb}(T_{air} + 273.2)^4 \quad (14)$$

where  $\epsilon_{atm}$  is the emissivity of the atmosphere [-],  $\theta_{VTS}$  is the 'view to the sky' coefficient [-] and  $\sigma_{sb}$  is Stefan-Boltzmann constant [ $W m^{-2} \circ C^{-1}$ ].

$$\epsilon_{atm} = 1.72 * \left(\frac{0.1 * e_a}{T_{air} + 273.2}\right)^{\frac{1}{2}} * (1 + 0.22 + C_L^2) \quad (15)$$

where  $C_L$  is the cloudiness [-] and  $e_a$  is the actual vapour pressure [kPa].

$$e_a = \frac{H}{100} e_s \quad (16)$$

where  $H$  is the relative humidity [%] and  $e_s$  is the saturation vapour pressure [kPa].

$$e_s = (6.1275e^{\left(\frac{17.27T_{air}}{237.3 + T_{air}}\right)}) \quad (17)$$

$$\varphi_{back\_radiation} = -0.96\sigma_{sb}(T + 273.2)^4 \quad (18)$$

$$\varphi_{land\_cover} = 0.96(1 - \theta_{VTS})0.96\sigma_{sb}(T_{air} + 273.2)^4 \quad (19)$$

Latent heat flow ( $\varphi_{evaporation}$ ) [ $W m^{-2}$ ] is calculated following the Penman equation for open water (Monteith, 1981):

$$\varphi_{evaporation} = -\rho_w L_e E \quad (20)$$

where  $L_e$  is the latent heat of evaporation [ $J kg^{-1}$ ] and  $E$  is the Penman open water evaporation [ $m s^{-1}$ ].

$$L_e = 1000(2501.4 + T) \quad (21)$$

$$E = \frac{s\varphi_r}{\rho_w L_e (s + \gamma)} + \frac{c_{air}\rho_{air}(e_s - e_a)}{\rho_w L_e r_a (s + \gamma)} \quad (22)$$

where  $s$  is the slope of the saturated vapour pressure curve at a given air temperature [ $kPa \circ C^{-1}$ ],  $\varphi_r$  is the net radiation [ $W m^{-2}$ ],  $\gamma$  is the psychrometric constant [ $kPa \circ C^{-1}$ ] and  $r_a$  is the aerodynamic resistance [ $s m^{-1}$ ].

$$\varphi_r = \varphi_{longwave} + \varphi_{solar} \quad (23)$$

$$r_a = \frac{245}{0.54v_{wind} + 0.5} \quad (24)$$

where  $v_{wind}$  is the wind velocity [ $m s^{-1}$ ].

$$s = \frac{4100e_s}{(237 + T)^2} \quad (25)$$

The equation for sensible heat flow ( $\varphi_{sensible\_heat}$ ) [ $W m^{-2}$ ] is given by [Boyd and Kasper \(2003\)](#):

$$\varphi_{sensible\_heat} = Br \varphi_{evaporation} \quad (26)$$

where Br is the Bowen ratio [-] given by:

$$Br = 6.1 * 10^{-4} P_A \frac{T - T_{air}}{e_s^w - e_a^w} \quad (27)$$

where  $P_A$  is the adiabatic atmospheric pressure [kPa],  $e_s^w$  and  $e_a^w$  are the saturated and actual vapour pressure using the stream temperature [kPa].

$$e_a^w = \frac{H}{100} e_s^w \quad (28)$$

$$e_s^w = 0.61275 e^{(\frac{17.27T}{237.3+T})} \quad (29)$$

$$P_A = 101.3 - 0.1055z \quad (30)$$

where  $z$  is the elevation [m] at which humidity and air temperature were measured.

Heat Exchange between the streambed and the stream  $\varphi_{bed}$  [ $W m^{-2}$ ] is computed by combining each stream cell with a vertical 1D streambed model ([Boyd and Kasper, 2003](#)):

$$\varphi_{bed} = -k \frac{T - T_{streambed}}{\frac{\Delta z}{2}} \quad (31)$$

Where  $k$  is the thermal conductivity of the combined water and soil matrix [ $J m^{-1} s^{-1} ^\circ C^{-1}$ ],  $T$  is the water temperature in the stream [ $^\circ C$ ],  $T_{streambed}$  is the temperature of the upper streambed cell of the streambed model [ $^\circ C$ ] and  $\Delta z$  is the thickness of the top-most cell [m]. Temperatures in the vertical 1D streambed model are solved using the advection-diffusion heat equation, with an upwind and a central difference solution for advection and diffusion respectively and a fixed cell size:

$$T_{iz}^{j+1} = T_{iz}^j + \frac{\Delta t}{c\rho} \left( \frac{k}{\Delta z^2} (T_{iz-1}^j - 2T_{iz}^j + T_{iz+1}^j) - \frac{v_z c_w \rho_w}{\Delta z} (T_{iz-1}^j - T_{iz}^j) \right) + \frac{R_{bed}}{\Delta z} \quad (32)$$

where  $T_{iz}^{j+1}$  is the groundwater temperature [ $^\circ C$ ] at grid cell  $iz$  at the new time level  $j + 1$ ,  $j$  denotes the old time level and  $iz - 1$  the grid cell above cell  $i$ ,  $v_z$  is the vertical groundwater flux (specific discharge) [ $m s^{-1}$ ],  $c$  and  $\rho$  are the specific heat and density of the combined water and soil matrix, and  $R_{bed}$  is a source/sink term which only applies to the top model layer which represents the streambed. This layer exchanges energy with the stream water and is heated by the fraction  $D_f$  of the solar radiation ( $\varphi_{solar}$ ) reaching the streambed. The source/sink term  $R_{bed}$  is given by:

$$R_{bed} = -\varphi_{bed} + \varphi_{solar} \frac{D_f}{1 - D_f} \quad (33)$$

The lower boundary of the model has a fixed temperature to represent a stable aquifer temperature at depth and the upper cell of the streambed model represents the stream and has a temperature that is updated every time step. Heat from streambed friction is considered to be negligible.

## 2.5. Model parameterization

The model was set-up for a length of 1500 m divided into 45 cells based on the flow velocity (Eq. (3)), and with characteristics similar to the Springendalse Beek such as springs, tributaries and groundwater-fed ponds. The model was run with a time step of 90 s for a total of three months: June and July 2016 to spin-up the model to get rid of artificial features inherited from the simple initial condition, and August 2016 for analysis. The vertical streambed models consisted of cells of 0.05 m and had a constant temperature boundary equal to the mean annual air temperature at a depth of 5 m. This depth could potentially be too shallow to have no seasonal temperature variations and we therefore ran a model test with the boundary at a depth of 10 m, but this did not result in a significant difference in stream temperature. The first cell was fed by seepage and an extra discharge component with the same temperature as the seepage in that cell, so that this discharge could be calibrated without getting unrealistic seepage rates through the small streambed area in the model cell. Air temperature, humidity, cloud cover and solar radiation were measured at nearby meteorological station Twenthe by the Dutch Meteorological Institute. The values that were used for thermal physical properties of the sediments were reported by [Anibas et al. \(2011\)](#) for another lowland stream with a sandy streambed and a wind velocity of  $0.1 m s^{-1}$  was taken from [Westhoff et al. \(2007\)](#), representing the wind-sheltered location of the stream in a dense forest with abundant plants growing in and around the stream.

## 2.6. Scenario modelling

Different scenarios were run with the calibrated model ([Table 3](#)). The effect of climate warming was tested by raising the air temperature by two degrees in scenario 1a, while keeping the temperature of the deeper groundwater the same. Because the increase in air temperature is expected to also increase the temperature of the groundwater (e.g. [Menberg et al., 2014; Taylor and Stefan, 2009](#)), in scenario 1b both the air and groundwater temperature were increased by  $2 ^\circ C$ . The importance of groundwater was tested by running the model with 50% more and 50% less groundwater seepage in the stream (scenarios 2 and 3). The effect of shading was evaluated by removing shading from a small part of the modelled stream (scenario 4) and by removing shading from the whole catchment (scenario 5).

## 3. Results

### 3.1. FO-DTS temperature measurements

#### 3.1.1. Springendalse Beek

[Fig. 3](#) displays results of temperature measurements in the Springendalse Beek in summer and winter. In summer, the absolute temperature slightly increases in the downstream direction ([Fig. 3b](#)) and the daily temperature amplitude tends to go up when there are no lateral inflows. Low temperatures between 10.3 and  $15.0 ^\circ C$  close to the spring area ( $x = 200$ ) indicate a strong influence of groundwater inflow. Downstream of the spring, the inflow of groundwater is less, and stream temperature is more influenced by atmospheric processes; measured temperatures vary between 12.3 and  $18.8 ^\circ C$  at  $x = 1450$  ([Fig. 3b](#)). In winter, the effect of groundwater seepage also is clearly visible in the DTS measurements. Upstream the stream water has a relatively high temperature in winter ( $5.0$ – $9.6 ^\circ C$ ), while temperatures decrease downstream ( $2.1$ – $6.6 ^\circ C$ ) ([Fig. 3e–g](#)). The mean and average daily standard deviation (SD) were also derived from the DTS data in order to locate groundwater seepage zones, using the fact that

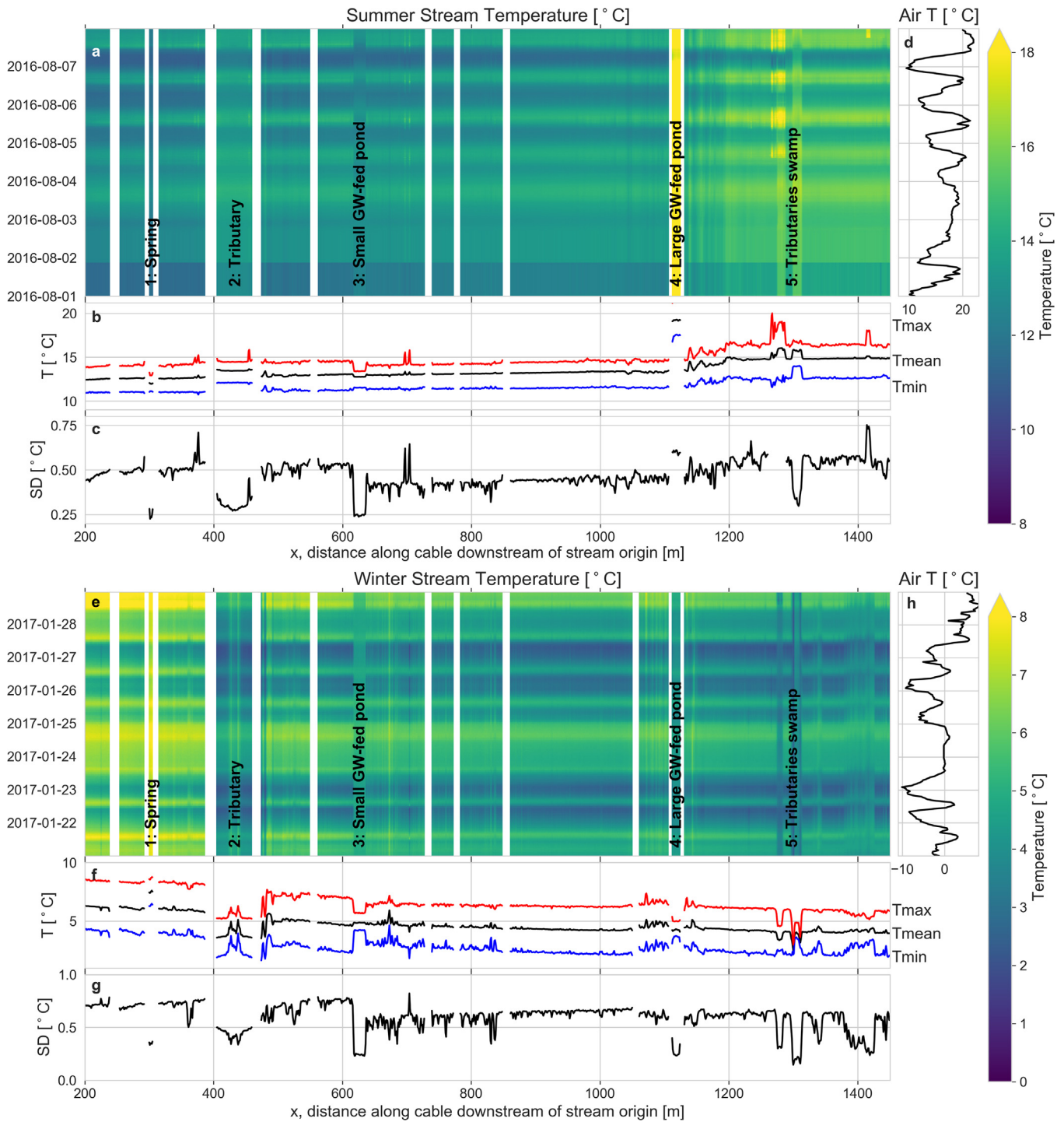


**Fig. 3.** Temperatures in the Springendalse Beek measured in a summer week (panels a–c) and in a winter week (panels e–g). Note that the legend colours are different between panels a and e. Streamflow is from left to right and the air temperature at a nearby meteorological station is given in panels d and h for the summer and winter period respectively. Maximum, average daily mean and minimum temperatures during the shown periods are given in panels b and f, and the average daily standard deviation in panels c and g. Thermal anomalies appear as warmer or colder vertical bands in panels a and e, of which locations 1–5 are indicated and listed in [Table 1](#). Locations where the cable was known to be exposed to the air are filtered out and appear as white vertical lines. (For interpretation of the references to colour in this figure legend, the reader is referred to the web version of this article.)

groundwater has less temperature variation and thus the SD is lowered at locations with seepage (e.g. [Hare et al., 2015](#); [Lowry et al., 2007](#); [Matheswaran et al., 2014a](#); [Rosenberry et al., 2016](#)). See for instance at  $x = 630$  and [Table 1](#), which summarizes the data for some specific locations. Upstream in the Springendalse Beek the SD is around  $0.5\text{ }^{\circ}\text{C}$  both in summer and winter, and in the

downstream direction increases in summer around  $1\text{ }^{\circ}\text{C}$  and remains approximately stable at  $0.5\text{ }^{\circ}\text{C}$  in winter.

[Table 1](#) lists characteristics of thermal anomalies associated with specific hydrological features such as tributaries and springs. At location 1 ([Fig. 3](#)) the cable was looped through the outflow of a small spring which had a lower summer and higher winter

**Table 1**  
Features in the Springendalse Beek with distinct thermal characteristics.

Location	Location along cable [m]	Feature	Summer		Winter		Observations
			Mean	SD	Mean	SD	
Upstream	200	–	12.6	0.75	6.3	1.02	
1	305	Spring	12.1	0.47	7.5	0.53	Sand volcanoes, loose sediment
2	435	Tributary	13.5	0.53	3.9	0.82	
3	630	Small GW-fed pond	12.8	0.43	4.9	0.36	Year-round discharge
4	1120	Large GW-fed pond	19.2	0.88	4.3	0.29	Year-round discharge
5	1300	Tributaries swamp	15.9	0.69	2.5	0.21	
Downstream	1430	–	15.0	0.88	3.9	0.94	

temperature than the water in the stream (Table 1) as a result of the stable temperature of groundwater seepage. The outflow of a small groundwater-fed pond at location 3 had this same thermal groundwater characteristics of lower summer and higher winter temperatures than the stream water. In addition, the stream temperature at  $x = 350, 650, 1100$  and  $1400$  m had similar characteristics as the spring (1) and the small groundwater-fed pond (3): the up- to downstream summer warming and winter cooling was dampened and SD values were lower than expected (Fig. 3). This suggests that significant seepage occurs at these locations. The outflow of a larger groundwater-fed pond at 4 had high summer temperatures and a high SD (Table 1), which is different from the small groundwater-fed pond and suggests a smaller groundwater influence on the temperature. This is potentially due to a longer residence time in the larger pond: although fed by groundwater, the larger volume of the pond results in a larger residence time of the water which slowly loses the groundwater thermal signal. Contrary to the groundwater indicative thermal signals, a tributary stream at location 2 (Fig. 3) had relatively high summer and low winter temperatures (Table 1), and the same holds for the outflow of a swamp through two small tributaries at location 5. The discharge of both

these inflows is fed by an agricultural area, where it derives from drains (shallow groundwater) and is influenced by atmospheric processes while flowing towards the Springendalse Beek.

Besides effects from groundwater seepage, effects of air temperature and rainfall are also visible in the DTS-measurements. For instance, a sharp increase in stream temperature occurred between August 1st and 2nd (Fig. 3a) and is the result of input from precipitation during a rainstorm. In addition, monitoring artefacts are shown, for instance around  $x = 1280$  where a temperature increase is seen from August 4th as a result of the cable becoming exposed to air due to lowering of the water level.

### 3.1.2. Elsbeek

The measured stream stretch in the Elsbeek is located further downstream from the stream origin than the measured stretch in the Springendalse Beek (approximately 5000 vs 200 m). The measured temperature of the Elsbeek slightly decreases in the downstream direction before increasing between  $x = 750$  and  $900$  and finally decreasing again towards the most downstream measured point (Fig. 4a, b). This pattern is also clearly visible in the SD (Fig. 4c), which is lower at locations with a lower temperature.

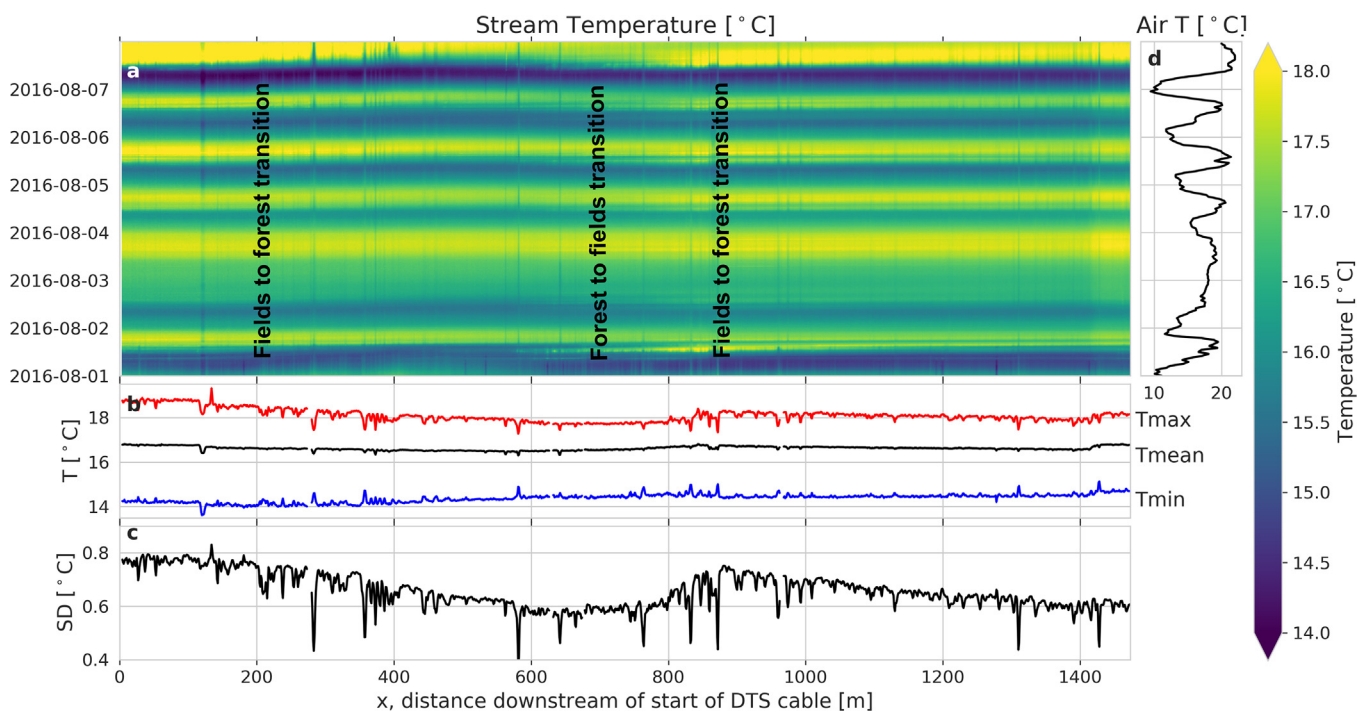


**Fig. 4.** Temperatures in the Elsbeek measured in a summer week (panel a). Streamflow is from left to right and the air temperature at a nearby meteorological station is given in panel d. Maximum, average daily mean and minimum temperatures during the shown period are given in panel b and the average daily standard deviation in panel c. Thermal anomalies appear as warmer or colder vertical bands in panel a.

The parts of the stream with decreasing temperatures coincide with the locations of (riparian) forests while the stretches with increasing temperatures are located in agricultural fields. The temperature measurements show several negative spikes in maximum temperature and SD (Fig. 4). While this appears similar to the characteristics of seepage, these locations have a minimum temperature significantly above the average groundwater temperature of around 11 °C. Instead of seepage, visual inspections showed that at these locations the DTS cable is either located on the bottom of (stagnant) pools or buried by sediment.

### 3.2. $^{222}\text{Rn}$ measurements

The  $^{222}\text{Rn}$  concentration in groundwater was measured both at piezometers within our catchment which showed concentrations between 3210 and 5800  $\text{Bq m}^{-3}$  and at the spring which showed

concentrations of 733 and 3730  $\text{Bq m}^{-3}$  (Fig. 5). The low spring concentration of 733  $\text{Bq m}^{-3}$  might be influenced by recent precipitation or by some decay in the spring area, as the other radon concentrations of 3000  $\text{Bq m}^{-3}$  and higher are in line with the concentrations found for groundwater in other studies in the Netherlands, including well fields in the region of our catchment (Kwakman and Versteegh, 2016; Yu et al., 2019). The  $^{222}\text{Rn}$  activity in the stream water in the most upstream part of the Springendalse Beek catchment is between 104 and 1240  $\text{Bq m}^{-3}$  while more downstream  $^{222}\text{Rn}$  concentrations are below 500  $\text{Bq m}^{-3}$  (Fig. 5), showing a decrease in groundwater influence in the downstream direction. The small groundwater-fed pond has a mean Radon level of 1388  $\text{Bq m}^{-3}$  ( $n = 4$ ) indicating a large relative influence of recent groundwater seepage. The concentrations in the large pond have an average of 177  $\text{Bq m}^{-3}$  ( $n = 3$ ; Fig. 5) indicating only a small influence of recent seepage.

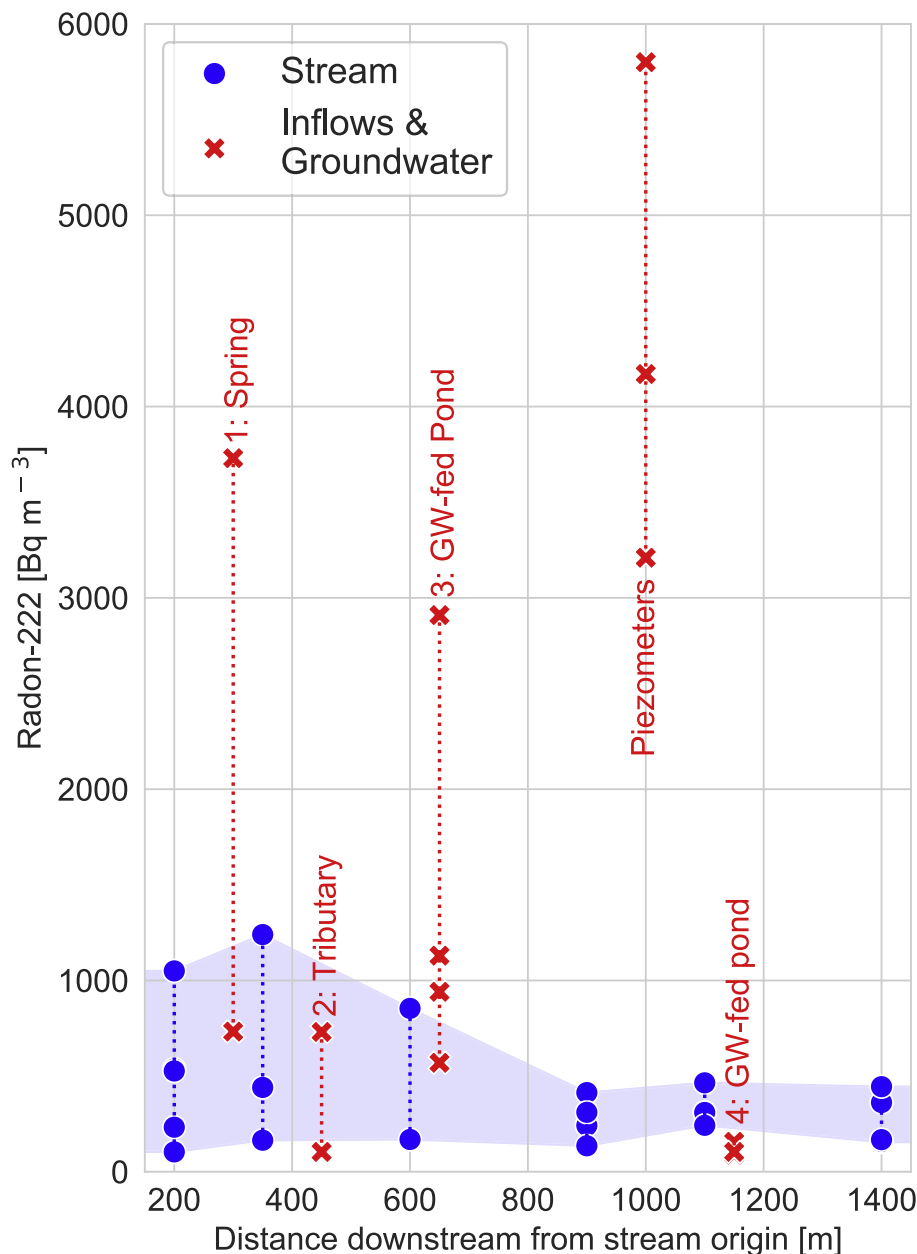


Fig. 5. Measurements of  $^{222}\text{Rn}$  taken during 6 field campaigns in the catchment of the Springendalse Beek: of stream water (blue circles) and of inflows towards the stream (Table 1) and piezometers (red crosses). (For interpretation of the references to colour in this figure legend, the reader is referred to the web version of this article.)

**Table 2**  
Calibrated model parameters.

Parameter	Description	Value	Reference
H [%]	Humidity 2016–2017	23–100	KNMI, Twenthe station
$T_{\text{air}}$ [°C]	Air temperature 2016–2017	–10.1 to 34.1	KNMI, Twenthe station
$\phi_{\text{inRad}}$ [ $\text{W m}^{-2}$ ]	Solar radiation 2016–2017	0.0–952.8	KNMI, Twenthe station
$\Delta t$ [s]	Time step	90	Chosen
$\Delta x$ [m]	Length of stream reservoir	Variable along x-axis	Based on Courant number = 1
$\Delta z$ [m]	Length of soil reservoir	0.05	Chosen
B [m]	Stream width	0.60–1.50	Estimated
Z [m]	Stream depth	0.03–0.07	Estimated
Q [ $\text{m}^2 \text{s}^{-1}$ ]	Stream discharge	0.05–0.34	Estimated
$v_z$ [ $\text{mm d}^{-1}$ ]	Groundwater flux	0.05–1.20	Estimated
$T_{\text{deepGW}}$ [°C]	Temperature of lower z boundary	11.0	Estimated
$D_{\text{diffuse}}$ [-]	Fraction of diffuse solar radiation	0.0	Estimated
$D_f$ [-]	Fraction of solar radiation reaching the streambed	0.5	Estimated
$R_{\text{SS}}$ [-]	Surface reflection	Based on solar angle	Boyd and Kasper (2003)
$C_s$ [%]	Shading factor	5–20	Estimated
$C_L$ [-]	Cloudiness	0–1	KNMI, Twenthe station
$\theta_{\text{VTS}}$ [-]	View to the sky coefficient	0.6	Estimated
$\sigma_{\text{sb}}$ [ $\text{Wm}^{-2} \text{ } ^\circ\text{C}^{-1}$ ]	Stefan-Boltzmann constant	$5.67 \cdot 10^{-8}$	–
$v_{\text{wind}}$ [ $\text{m s}^{-1}$ ]	Wind velocity	0.1	Westhoff et al. (2007)
$\gamma$ [ $\text{kPa } ^\circ\text{C}^{-1}$ ]	Psychrometric constant	0.66	Westhoff et al. (2007)
$\rho_a$ [ $\text{kg m}^{-3}$ ]	Density of air	1.2	–
$\rho_w$ [ $\text{kg m}^{-3}$ ]	Density of water	1000	–
$\rho_{\text{sed}}$ [ $\text{kg m}^{-3}$ ]	Density of the saturated sediment	1965	Anibas et al. (2011), Dujardin et al. (2014)
$c_{\text{air}}$ [ $\text{J kg}^{-1} \text{ } ^\circ\text{C}^{-1}$ ]	Specific heat capacity of air	1004	–
$c_w$ [ $\text{J kg}^{-1} \text{ } ^\circ\text{C}^{-1}$ ]	Specific heat capacity of water	4182	–
$c_{\text{sed}}$ [ $\text{J kg}^{-1} \text{ } ^\circ\text{C}^{-1}$ ]	Specific heat capacity of the saturated sediment	1365	Anibas et al. (2011), Dujardin et al. (2014)
$k_w$	Thermal conductivity of water	0.6	–
$k_{\text{sed}}$	Thermal conductivity of the saturated sediment	1.833	Anibas et al. (2011), Dujardin et al. (2014)

### 3.3. Model calibration

The manual calibration was done step-wise and an overview of the model parameters is shown in Table 2. The model is most sensitive to the parameters  $\theta_{\text{VTS}}$ ,  $D_{\text{diffuse}}$ , upstream starting Q and the width of the stream, and therefore focus was on these parameters during calibration. Discharge from groundwater seepage and lateral inflow, stream width and depth and shading varied along the stream length and were estimated using our knowledge of the field sites and were then further calibrated (Fig. 6). The initial

temperature of the stream and the streambed were set to 10 and 11 °C respectively. Calibration of  $D_f$  and  $D_{\text{diffuse}}$  resulted in values of 0.5 and 0.0 respectively. Lateral inflow from an agricultural stream was added to the model at  $x = 435$ . The temperature of this inflow represented discharge from a tile drained area (seepage from 1 m depth). The two seepage ponds in the Springendalse Beek were located at locations  $x = 650$  and 1150 m in the model. The pond sizes, depths, shading and seepage rates were also calibrated with the DTS measurements. Their depths were 1.5 and 1.0 m and their surface areas 900 and 3000  $\text{m}^2$  respectively. The pond at

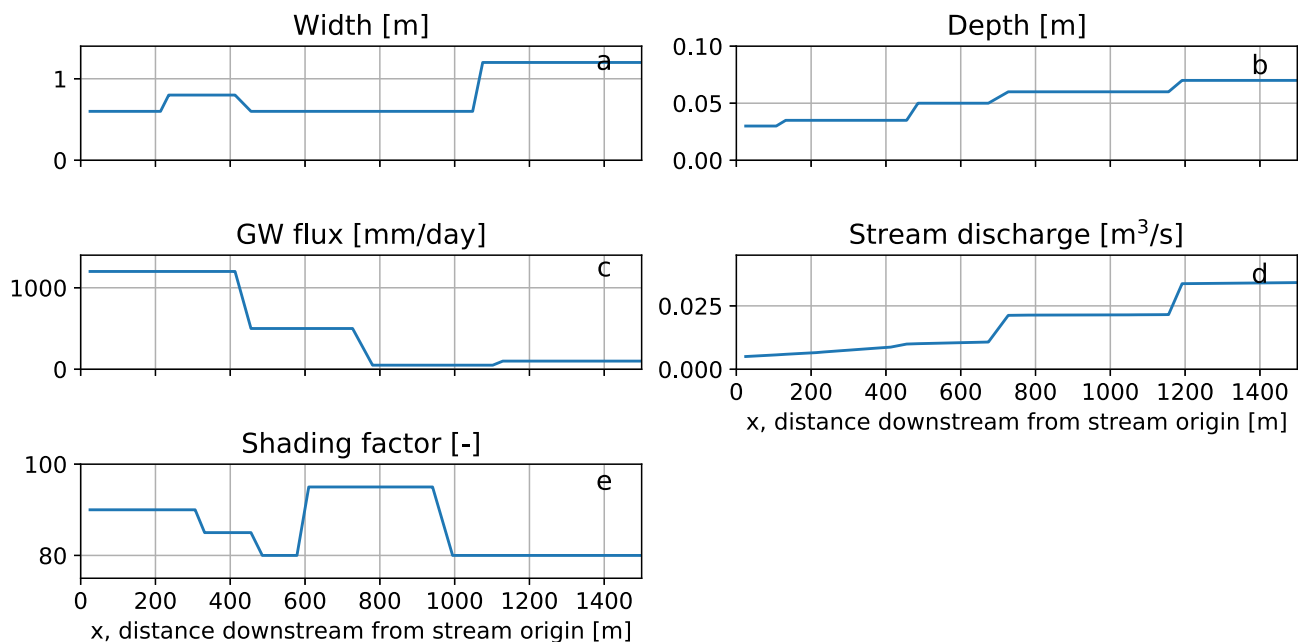


**Fig. 6.** Calibrated stream width (a) and depth (b), groundwater seepage rates (c), discharge (d) and shading factor (e) in the model, representing the Springendalse Beek.

650 m had a calibrated seepage rate of 1000 mm per day and was 90% shaded. The pond at 1150 m had a calibrated seepage rate of 350 mm per day and was not shaded with a shading factor of only 10%.

### 3.4. Modelled temperature distribution along the stream

The calibrated STM-GW model, using the parameters listed in Table 2, shows a reasonable fit with the observed DTS data from the Springendalse Beek (Fig. 7), especially considering that the model does not include local heterogeneity in e.g. water depth and air temperature. Both the diurnal temperature variation in the up- and downstream temperature are represented well by the model, although the simulated temperature upstream is slightly underestimated (Fig. 7b). Fig. 7c shows the modelled result for two night and two days (2 AM and 2 PM), for a warmer day (Day 1) and colder day (Day 2). The temperature pattern from up- to downstream on these days is simulated adequately by the model including the modelled features such as the spring and tributary spring. Especially the temperature step resulting from the tributary stream at  $x = 450$  and the inflow of water from the seepage ponds ( $x = 700$  and  $x = 1200$ ) lead to clear temperature steps in the model, that were also observed in the DTS measurements (Fig. 7c).

Using the model, we were able to investigate the theoretical importance of the different processes affecting the stream temperature. For comparison with the other energy fluxes, the heat energy provided by seepage [ $\text{W m}^{-2}$ ] was calculated using:

$$E_{\text{seepage}} = \Delta T v_z C_w \rho_w \quad (34)$$

where  $\Delta T$  is the temperature difference between the stream and seeping groundwater, which means that Eq. (34) gives the energy

flux compared to the current stream water temperature and is thus an *apparent* rather than an absolute heat flux, as explained by Kurylyk et al. (2016). Fig. 8 shows the modelled energy fluxes to and from the stream on August 6, 2016. The energy flux from seepage is mostly negative because seepage of groundwater often leads to cooling on summer days. The higher seepage rates given to the upstream part of the model are also shown in the energy fluxes (Fig. 8a and c): higher seepage rates lead to more cooling of the stream both through the advective flux and through increased streambed conduction. The negative energy fluxes from both bed conduction and seepage increase during the day, because stream water is heated and the temperature difference between seepage and stream water increases. The flux from solar radiation naturally has a day-night fluctuation and is lower at locations with shading. Sensible heat flow is dependent on the difference between stream water and air temperature (Eq. (27)) and therefore shows a day-night pattern as well. It decreases in the downstream direction, as the difference between stream water and air temperature decreases due to the heating or cooling of the stream water in the downstream direction by atmospheric processes.

### 3.5. Scenario modelling

From the base run (Fig. 7), several model parameters were changed to simulate different scenarios to get a better understanding of the possible future changes resulting from climate change and the role of groundwater in this. Table 3 shows the upstream ( $x = 200$ ) and downstream ( $x = 1450$ ) average, minimum and maximum stream temperature for the calibrated base run and five different scenarios.

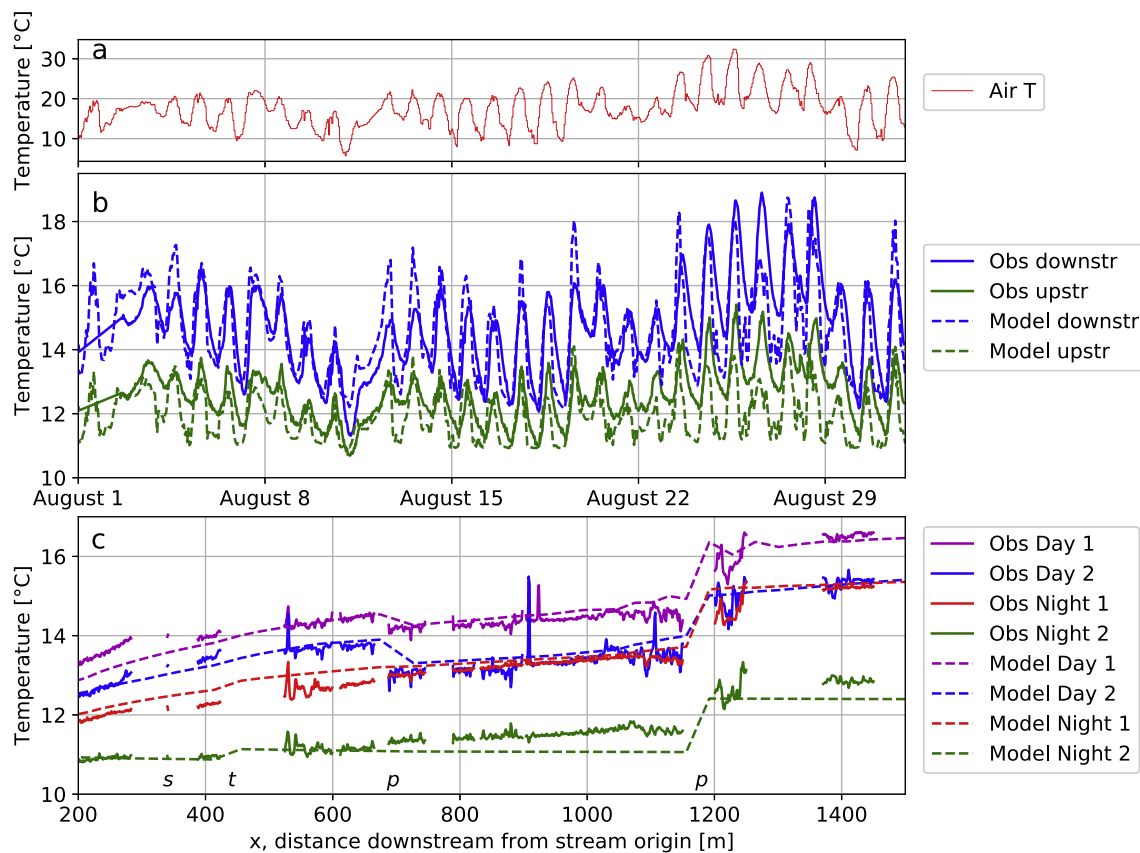


**Fig. 7.** Fit between the calibrated model and measurements taken in the Springendalse Beek in August 2016. Panel a shows the air temperature, panel b shows the fit for both up- ( $x = 200$ ) and downstream ( $x = 1450$ ) and panel c shows the fit for 2 day and 2 night measurements. The letters at the bottom of panel c indicate the location of a spring (s), a tributary (t) and ponds (p).

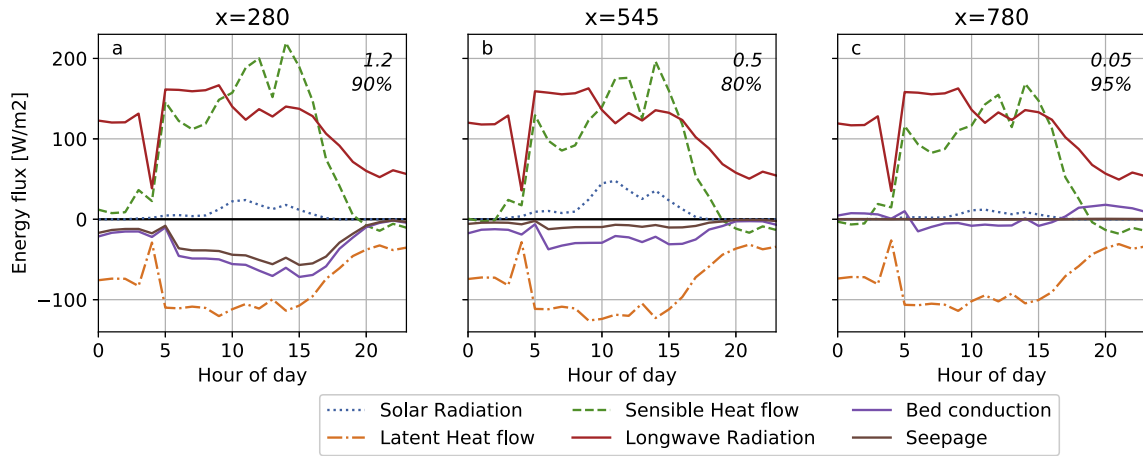


**Fig. 8.** Modelled energy fluxes to (positive) and from (negative) the stream at 3 different locations on August 6th 2016. The seepage rate ( $\text{m d}^{-1}$ ) and percentage of shading are indicated at the top right of the figures: panels a, b and c show locations with a high, medium and low seepage rate respectively.

**Table 3**  
Results of the scenario modelling: statistics for the month August 2016.

Scenario		Upstream temperature [ $^{\circ}\text{C}$ ]			Downstream temperature [ $^{\circ}\text{C}$ ]		
		Average	Min	Max	Average	Min	Max
0	Base run	12.0	10.9	14.3	14.6	12.2	18.7
		Temperature change from base run [ $^{\circ}\text{C}$ ]:					
1a	T + 2 $^{\circ}\text{C}$ , GWlower_boundary + 0 $^{\circ}\text{C}$	0.3	0.0	0.5	0.8	0.2	1.0
1b	T + 2 $^{\circ}\text{C}$ , GWlower_boundary + 2 $^{\circ}\text{C}$	1.9	2.0	1.8	2.0	2.0	1.9
2	50% more GW in stream	-0.1	0.0	-0.3	-0.1	-0.1	-0.2
3	50% less GW in stream	0.3	0.0	0.8	0.4	0.0	0.7
4	No shading between x = 450-500	0.0	0.0	0.0	0.1	0.0	0.2
5	No shading	1.2	0.0	5.0	1.1	0.0	4.3

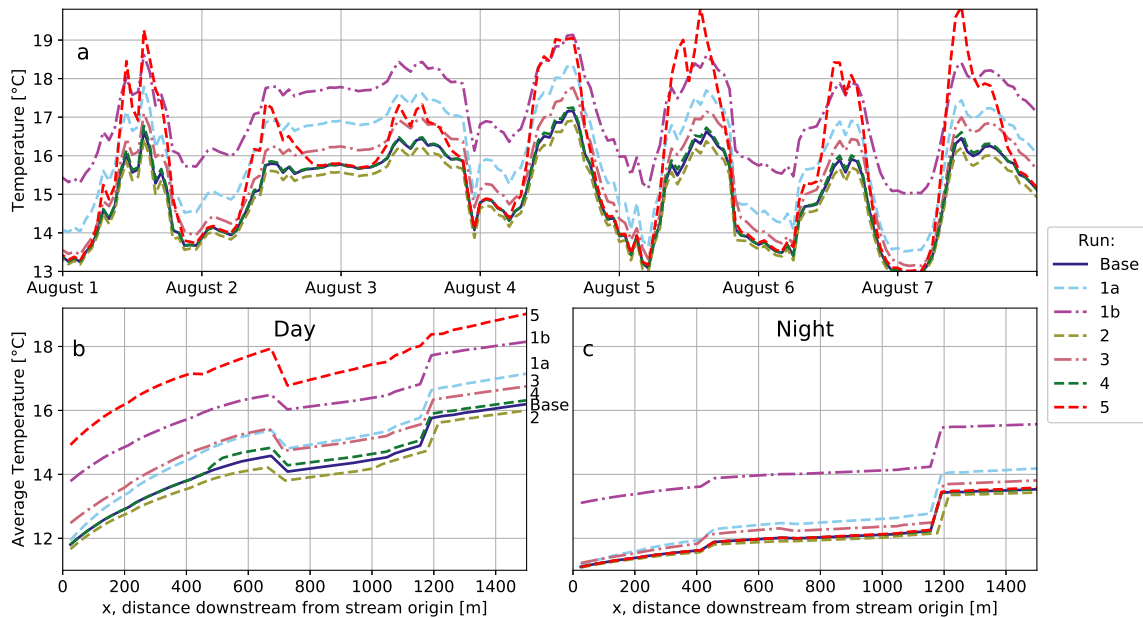


**Fig. 9.** Result of the modelled scenarios listed in Table 3. Panel a shows the downstream ( $x = 1450$ ) temperature simulated in the different scenario runs for the whole of August 2016. Panels b and c show the simulated mean day and night temperature (August 2016) from up to downstream.

An increase in air temperature in scenarios 1a and 1b resulted in an increase in water temperature (Fig. 9a). In scenario 1a a stable groundwater temperature buffers the increase in water temperature compared to scenario 1b, where the stream temperature increased by approximately the same amount as the air and

groundwater temperature (Table 3, Fig. 9a). The upstream temperature is hardly affected by an increase in air temperature because it is located close to the upstream stream spring. Especially the night temperature both up- and downstream seems to be almost fully determined by the groundwater temperature, as the 2  $^{\circ}\text{C}$  increase

of the lower boundary in scenario 1b leads to a similar increase of the minimum temperature both upstream and downstream. Scenarios 2 and 3 show the effect of an increase or decrease of groundwater seepage in the stream: an increase of seepage resulted in lower maximum temperatures while a decrease resulted in higher maximum temperatures (Table 3). The removal of shading between  $x = 450$  and  $500$  had a local effect on this new non-shaded part where temperature increased by  $0.4\text{ }^{\circ}\text{C}$  (Fig. 9b), and had only a slight effect on the maximum temperature downstream ( $+0.1\text{ }^{\circ}\text{C}$ ). In scenario 5, where shading was removed from the whole stream, daytime temperatures strongly increased, approximately the same or more as in scenario 1b. However, night temperatures stayed the same since the effect of shading is depleted when there is no solar radiation (Fig. 9).

## 4. Discussion

### 4.1. Mapping local and diffuse groundwater seepage

#### 4.1.1. Springendalse Beek

The stream temperature and  $^{222}\text{Rn}$  measurement in the Springendalse Beek reflected the stream to be highly influenced by groundwater, as was expected from the fact that several springs exist in this particular catchment (van der Aa et al., 1999). The stream had both local and diffuse seepage locations. Two local seepage spots were identified from the temperature measurements: a spring and groundwater-fed pond (locations 1 and 3; Table 1). The  $^{222}\text{Rn}$  measurements and other field observations such as sand volcanoes, loose sediments, abundant presence of macrofauna and year-round discharge confirmed the presence of seepage at these features (Fig. 5). Small hotspots of diffuse seepage (maximum length a few meters) were located at 4 locations (around  $x = 350, 650, 1100$  and  $1400$ ), indicated by lower SD values and a dampening of the warming in summer and cooling in winter in the downstream direction. However, the hotspots were not clearly visible in the  $^{222}\text{Rn}$  measurements, probably because their flux was too small compared to river discharge to influence  $^{222}\text{Rn}$  downstream. The observed increase in discharge in the downstream direction indicates that low rates of diffuse seepage are occurring in the catchment, but this could not be shown in the measurements, as small fluxes cannot be located adequately using DTS (e.g. Krause et al., 2012) or  $^{222}\text{Rn}$  measurements. Substantial variations in time were found between the  $^{222}\text{Rn}$  measurements, which could be related to changes in exchange with the atmosphere due to wind and turbulence (e.g. Cartwright et al., 2014; Cook, 2013; Genereux and Hemond, 1992; Wallin et al., 2011) or to changing flow velocities and discharge leading to a change in decay time.

The outflow of the small pond and the measured groundwater (spring and piezometers) have a clear groundwater  $^{222}\text{Rn}$  signal which is much higher than the  $^{222}\text{Rn}$  values measured in the outflow of the large groundwater-fed pond (Fig. 5). It was expected that both ponds would show a clear groundwater signal because both have a year-round discharge but no inflow of surface water and therefore must have a significant input of groundwater. The  $^{222}\text{Rn}$  concentration at the large pond is the lowest measured in the catchment and was at some occasions difficult to detect (Fig. 5). The difference in  $^{222}\text{Rn}$  between the ponds suggests that the residence time of water in the large pond is much larger than in the small pond, allowing for more decay of Radon and a change in the thermal signature. With a half-life time of 3.8 days and ignoring degassing for simplicity, seeping groundwater with a  $^{222}\text{Rn}$  concentration of  $3500\text{ Bq m}^{-3}$  (as measured in the piezometers and spring) would take approximately 5 days to reach the average level of  $1400\text{ Bq m}^{-3}$  found in the small pond but 19 days

to reach the average level of  $117\text{ Bq m}^{-3}$  found in the large pond. Relating the residence time with the volume and discharge in the pond is done using:

$$T = \frac{V}{N} \quad (35)$$

where  $T$  is the characteristic time [days],  $V$  is the volume [L] and  $N$  is the (groundwater) recharge [ $\text{L s}^{-1}$ ] (e.g. van Ommen, 1986). The outflow of the pond can be assumed to equal the groundwater discharge towards the ponds and was measured at  $4$  vs  $3\text{ L s}^{-1}$  for the large and small pond respectively. With estimated volumes of  $5000$  and  $1300\text{ m}^3$  respectively, the characteristic residence time is estimated to be 15 and 5 days, and thus close to the estimations of 19 and 5 days using  $^{222}\text{Rn}$ . The slight deviation found for the large pond could result from an underestimation of pond volume, but also from ignoring the atmospheric exchange of radon, which would also lead to a decrease in the estimated residence time. However, we assume atmospheric exchange to be a much slower process than radioactive decay in the ponds, especially because they contain stagnant water, are located in a forest and thus sheltered from wind and contain abundant water plants that prohibit the presence of waves or turbulence that would promote the atmospheric exchange. As atmospheric exchange would then be governed by diffusion from deeper water to the pond surface, this effect was assumed to be negligible relative to the effect of the radioactive decay with a half-life time of 3.8 days (e.g. Dimova et al., 2013; Dulaiova and Burnett, 2006; Emerson and Broecker, 1973; Zappa et al., 2003). The longer residence time in the large pond than in the small pond results in more warming in summer (Table 1), especially since the large pond is barely shaded.

#### 4.1.2. Elsbeek

It was not possible to locate groundwater seepage in the Elsbeek using the FO-DTS measurements. An increase in streamflow and the presence of iron oxide precipitation along banks show that diffuse seepage does occur in the catchment but apparently these fluxes are not large enough to create a distinguishable temperature signal. Patterns in the measured temperature were attributed to morphological and riparian differences. Several thermal anomalies were found but were caused by the burial of sediment and presence of pools. In addition, the temperature and SD along the stream seem to have a good correlation with the sequence of open-shaded-open-shaded stream stretches (Fig. 4).

### 4.2. DTS-measurements in a heterogeneous stream system

Similar to the conclusions of Matheswaran et al. (2014a), the standard deviation of diurnal temperatures was found to be best suitable for locating groundwater seepage in summer, while the mean temperature appeared useful for winter measurements. Several difficulties appeared in analysis of the DTS measurements. First, the DTS cable and streambed may be warmed up by direct solar radiation (Neilson et al., 2010), although we did not find evidence for this. Second, sedimentation of the DTS cable led to a similar signal as seepage, which was also found by e.g. Karan et al. (2017). Sediment functions as insulation of the cable which therefore shows a buffered temperature signal. To separate the temperature effect of sedimentation, Sebok et al. (2015) used parallel DTS cables which allowed them to detect sedimentation and scouring. Hilgersom et al. (2016) were able to distinguish sedimentation by applying a 3D DTS device, although this seems only practical for lab or small field areas. Third, we aimed to place the cable in the centre of the stream but because of that may have missed seepage occurring only on certain sides of the stream, as recent studies have shown the large heterogeneity in shallow subsurface

temperatures, groundwater flow paths and seepage (e.g. Gilmore et al., 2016; Kennedy et al., 2009; Rosenberry et al., 2016).

Lastly, measurements from the Elsbeek suggested that stratification of water temperatures (Neilson et al., 2010) is occurring in pools (Fig. 4), also leading to a temperature signal similar to that of seepage. These pools in the Elsbeek are deep (~1 m) compared to the low streamflow in summer (can go to zero in dry periods). Because the fibre-optic cable is placed on the streambed, the temperature of the water at the bottom of a pool is measured. Because more energy is needed to heat the water mass in a pool, the temperature reacts more slowly on changes and thus pools present a buffered temperature signal, similar to the effect of groundwater seepage. The temperature at the pool bottom can significantly differ from the temperature of the surface as thermal layering can occur in deeper pools, where solar radiation does not heat the entire water column (Sebok et al., 2013). Pools do not necessarily greatly influence the temperature of streams, as this stratification can only occur if the water flowing into the pool stays at the surface and continues to flow in the downward direction, with limited mixing with the water in the pool. Sedimentation of the cable at the bottom of the pool may also occur, further buffering the measured temperature signal.

#### 4.3. The buffering capacity of shading and stream morphology

Compared to other studies (e.g. Harrington et al., 2017), the effect of direct solar radiation on the temperature of our study stream is relatively low and the other fluxes relatively high (Fig. 8). Direct solar radiation does not affect stream temperatures as much as the other atmospheric energy fluxes because of the high shading of the Springendalse Beek. In addition, the other energy fluxes are relatively high because the temperature difference between the stream water and air is large, increasing e.g. longwave radiation (Equation (19)). As expected, shading reduced maximum stream temperatures (Table 3, Fig. 9). However, shading has a large impact on the temperature of the stream: without shading, the water temperature would increase in summer by ~4 °C (scenario 5). Removing shading from a small stream stretch (50 m) affected the maximum temperature even 1 km downstream (scenario 4; Fig. 9b). Garner et al. (2014) argued that while shading seems to cause cooling of stream water, the discrepancy between the water temperature in open and shaded stretches is caused by the fact that in shaded parts water is less heated and daytime heating therefore lags behind compared to non-shaded parts. This could also explain the observed temperature variation between open and shaded parts in the Elsbeek, where temperatures increase in the non-shaded parts and decrease in the shaded parts (Fig. 4).

In addition to shading, the stream temperature is also influenced by the water depth. A shallow stream warms up faster, but also has a higher flow velocity than locations with pools allowing less time for warming of the water. The temperature measured in the Elsbeek showed that the temperature at the bottom of deeper pools was buffered and had less extreme temperature peaks than the surrounding stream sections because the larger body of water at these locations was able to adsorb more heat than shallow stream sections.

#### 4.4. Temperature buffering by groundwater

Our temperature measurements showed that groundwater provides relatively cool water in summer and warm water in winter (Figs. 4 and 5), which was especially clear in springs (Table 1). Separating the energy fluxes of seepage from the other processes using the model (Fig. 8) showed that the importance of groundwater for stream temperature depends on the temperature difference between the surface- and groundwater. For instance, the buffering

capacity of seepage increases during a summer day as the stream gets heated and the temperature difference increases (Fig. 8). The scenarios showed that the increase in stream temperature resulting from decreased seepage (scenario 3) is larger than the decrease in temperature following from increased seepage (scenario 2). This is not only due to the change in the amount of groundwater versus the volume of stream water, but also follows from the fact that with higher groundwater fluxes the temperature of seepage is more similar to the deeper groundwater than with low seepage rates, because less time is available for downward conduction of heat. Higher seepage fluxes thus increase the temperature gradient in the streambed, and therefore increase the buffering capacity of groundwater both through the advective flux and through increased streambed conduction (Caissie and Luce, 2017).

Recent studies showed the importance of 'source depth' of seepage for the temperature signal that is transported by groundwater to surface waters (Briggs et al., 2018a, 2018b; Kurylyk et al., 2015). The temperature of shallow groundwater is influenced by the seasonality at the surface, and as such the buffering capacity of this groundwater is lower than that of deeper groundwater. Thus, groundwater seepage may hold a (lagged and attenuated) seasonal temperature signal, resulting from either the groundwater flow path and transferred from infiltration zones (Briggs et al., 2018b, 2018a; Kurylyk et al., 2015) or from heat conduction from the streambed at the seepage zone (Caissie and Luce, 2017). Our study did include the second process of heat conduction at seepage zones (Eq. (32)), which is especially important if seepage velocities are slower and deep flow paths are dominant. However, with the methods in our study we were not able to consider the first process of source depth, which is especially important when groundwater velocities are high and/or travel times short, which is known to be the case for at least part of the seepage in these catchments (Kaandorp et al., 2018a).

We found that the spring and two groundwater-fed ponds discharge groundwater towards the stream, but with different residence times from the moment of seepage till the moment of discharge to the stream. This leads to a clear difference in the temperature effect on the stream, which is listed in Table 4. Because the water discharging through the spring only takes little time to join the stream, its temperature in winter is always higher than the stream water (Fig. 3). As residence time increases, the water is more influenced by atmospheric processes such as sensible heat flow and it changes temperature compared to the stream water. For instance, the large groundwater-fed pond has an estimated residence time between 15 and 19 days and in winter discharges water towards the stream which is both colder on average and during the day (maximum) than the water in the stream.

#### 4.5. Climate warming

Scenarios 1a and 1b, in which air temperatures were increased in both scenarios and groundwater temperatures only in scenario 1b, showed how the buffering capacity of groundwater highly depends on the temperature increase of groundwater in a changing climate. Much is still unknown about the exact response of the temperature of groundwater to climate change (e.g. Menberg et al., 2014; Watts et al., 2015). Kurylyk et al. (2015) simulated the temperature of shallow groundwater during several climate change scenarios. They showed for instance a case where 50 years after an instantaneous increase in the air temperature of 2.0 °C the temperature of groundwater at a recharge location in a sandy aquifer had increased by 1.9 °C at a depth of 5 m and by 1.6 °C at a depth of 20 m. Because it is expected that the increase in the groundwater temperature will always lag behind on the increase of the air temperature (e.g. Kurylyk et al., 2013), the temperature difference between the two increases in a warming climate,

**Table 4**  
Comparison of features with point groundwater seepage.

		Spring	Small GW-fed pond	Large GW-fed pond
Location		1	3	4
Location along cable		305 m	630 m	1120 m
Residence time/time since seepage		0–1 days	5 days	15–19 days
Temperature in winter relative to stream temperature	Minimum	↑	↑	↑
	Average	↑	↑	↓
	Maximum	↑	↓	↓

depending on the depth where groundwater is flowing. This would lead to a relative increase in the buffering capacity of groundwater compared to the current climate and thus partly buffers the effect of climate warming in groundwater dominated streams.

Climate change might not lead to a consistent year-round increase in temperatures, but instead lead to a different temperature increase in summer than in winter, which will also affect the buffering capacity of groundwater on stream temperature. In our study area, part of the streamflow is derived from deeper groundwater (Kaandorp et al., 2018a) and the temperature of this deeper groundwater depends on the average temperature increase, not seasonality as seasonal signals are dampened with depth. Therefore, if summer temperatures increase more than winter temperatures (e.g. by 3 °C and 1 °C respectively) and the groundwater temperature increases by the average (e.g. 2 °C), the temperature difference between the stream and groundwater changes. In this example the thermal buffering by groundwater is increased both in summer and winter compared to in the current climate. However, if the reverse happens and winter temperatures increase more than summer temperatures, the buffering capacity of groundwater decreases. Furthermore, climate change also leads to changes in cloudiness and humidity, affecting direct solar radiation and latent heat flow and thus both stream and groundwater temperatures (Taylor and Stefan, 2009). We conclude that the effect of climate warming on groundwater temperatures is extremely complex and can have large spatial heterogeneity due to differences in e.g. recharge rates (Kurylyk et al., 2014) and geohydrological settings.

#### 4.6. Implications for groundwater-dependent streams and ecology

The temperature of groundwater is likely to be lower than maximum air temperatures in summer and thus in most climate warming scenarios seepage buffers temperature peaks. In addition, groundwater dominated streams have a lower risk of drying up than other streams and rivers, and are therefore able to support the survival of species during drought. Springs especially, can deliver a thermal signal most related to groundwater towards the stream due to their local high flow velocities, which does not allow much time for downward heat conduction. Groundwater-fed streams are less vulnerable to climate change thanks to these less intense temperature and discharge extremes.

However, the thermal refugia created by groundwater seepage are still threatened by climate warming, as many species living at these locations are more susceptible to changes in temperatures than species that are already adapted to more variable water temperatures (e.g. Hazelwood and Hazelwood, 1985; van den Hoek and Verdonchot, 2001). If future temperatures rise, the input flux of groundwater might not be high enough to ensure the required low temperature certain species need to survive (e.g. Kurylyk et al., 2014). The high groundwater input into the Springendalse Beek allows for the presence of spring and spring stream species (Verdonchot, 1990) and a high amount of rare species (van Walsum et al., 2002). This, together with the high amount of shad-

ing makes this stream a special case especially for the Netherlands and worth protecting.

## 5. Conclusions

Several measurement techniques were combined with a stream temperature model in order to study the importance of groundwater on the temperature of lowland streams. Using DTS measurements, localized seepage was mapped in two Dutch streams, which was confirmed by sampling of <sup>222</sup>Rn. We have seen that groundwater seepage is able to buffer the temperature of stream and provide thermal and climate refugia by lowering maximum temperatures. Seasonality in seepage temperatures can be caused by shallow and fast flow paths from infiltration areas or by heat conduction in seepage zones with slow groundwater velocities. Our measurements suggest that while air temperature and shading generally have a large influence on stream temperature, the presence of significant seepage can be crucial in the occurrence of thermal refugia. The effect of groundwater may be even more important in a warming climate, although this depends on the exact change in air temperature and its seasonality. We conclude that groundwater dominated streams are potentially more climate resilient than streams without a significant contribution from seepage. It seems possible to make use of groundwater in reducing summer temperature maximums, as an alternative or additionally to the creation of (riparian) shading. For instance, reducing the pumping of groundwater can increase groundwater levels and seepage. More research effort is needed on the exact consequence of climate change on the temperature of groundwater and therefore of seepage, as this is still mostly unclear and depends on many (local) factors. We conclude with the statement that groundwater seepage is a crucial factor to include the study and management of lowland stream temperatures and ecology.

## Declaration of interests

The authors declared that there is no conflict of interest.

## Acknowledgements

We thank Stèphanie de Hilster for her help in obtaining and processing the field data and Liang Yu for help with the Radon measurements. The assistance of Mike van der Werf, Hendrik Kok, Edvard Ahlrichs and Bert Woertink in taking the measurements was also appreciated. We are grateful to Huite Bootsma for his valuable input in the modelling procedure. We thank Rob van Dongen and colleagues from Staatsbosbeheer for granting us access to the Springendalse Beek nature reserve and Roel Korbee and Hans Slot for providing a place for the measurement equipment on their property. We also thank three anonymous reviewers for their valuable comments on the manuscript. This work is part of the MARS project (Managing Aquatic ecosystems and water Resources under multiple Stress) funded under the 7th EU

Framework Programme, Theme 6 (Environment including Climate Change), contract 603378 (<http://www.mars-project.eu>).

## References

- Anibas, C., Buis, K., Verhoeven, R., Meire, P., Batelaan, O., 2011. A simple thermal mapping method for seasonal spatial patterns of groundwater-surface water interaction. *J. Hydrol.* 397, 93–104. <https://doi.org/10.1016/j.jhydrol.2010.11.036>.
- Benoit Bovy, & Geordie McBain. (2017, November 20). benbovy/xarray-simlab: 0.1.1 (Version 0.1.1). Zenodo. <https://doi.org/10.5281/zenodo.1063391>.
- Bense, V.F., Kooi, H., 2004. Temporal and spatial variations of shallow subsurface temperature as a record of lateral variations in groundwater flow. *J. Geophys. Res. B: Solid Earth* 109, 1–13. <https://doi.org/10.1029/2003JB002782>.
- Bowes, M.J., Loewenthal, M., Read, D.S., Hutchins, M.G., Prudhomme, C., Armstrong, L.K., Harman, S.A., Wickham, H.D., Gozzard, E., Carvalho, L., 2016. Identifying multiple stressor controls on phytoplankton dynamics in the River Thames (UK) using high-frequency water quality data. *Sci. Total Environ.* 569–570, 1489–1499. <https://doi.org/10.1016/j.scitotenv.2016.06.239>.
- Boyd, M., Kasper, B., 2003. Analytical methods for dynamic open channel heat and mass transfer: methodology for the heat source. *Model Version 7*, 204.
- Briggs, M.A., Johnson, Z.C., Snyder, C.D., Hitt, N.P., Kurylyk, B.L., Lautz, L., Irvine, D.J., Hurley, S.T., Lane, J.W., 2018a. Inferring watershed hydraulics and cold-water habitat persistence using multi-year air and stream temperature signals. *Sci. Total Environ.* 636, 1117–1127. <https://doi.org/10.1016/j.scitotenv.2018.04.344>.
- Briggs, M.A., Lane, J.W., Snyder, C.D., White, E.A., Johnson, Z.C., Nelms, D.L., Hitt, N.P., 2018b. Shallow bedrock limits groundwater seepage-based headwater climate refugia. *Limnologia* 68, 142–156. <https://doi.org/10.1016/j.limno.2017.02.005>.
- Briggs, M.A., Lautz, L.K., McKenzie, J.M., Gordon, R.P., Hare, D.K., 2012. Using high-resolution distributed temperature sensing to quantify spatial and temporal variability in vertical hyporheic flux. *Water Resour. Res.* 48, 1–16. <https://doi.org/10.1029/2011WR011227>.
- Caisse, D., Luce, C., 2017. Quantifying streambed advection and conduction heat fluxes. *Water Resour. Res.* 53, 1595–1624. <https://doi.org/10.1002/2016WR019813>.
- Cartwright, I., Hofmann, H., Gilfedder, B., Smyth, B., 2014. Understanding parafluvial exchange and degassing to better quantify groundwater inflows using <sup>222</sup>Rn: the King River, southeast Australia. *Chem. Geol.* 380, 48–60. <https://doi.org/10.1016/j.chemgeo.2014.04.009>.
- Cook, P.G., 2013. Estimating groundwater discharge to rivers from river chemistry surveys. *Hydrol. Process.* 27, 3694–3707. <https://doi.org/10.1002/hyp.9493>.
- Cook, P.G., Lamontagne, S., Berhane, D., Clark, J.F., 2006. Quantifying groundwater discharge to Cockburn River, southeastern Australia, using dissolved gas tracers <sup>222</sup>Rn and SF<sub>6</sub>. *Water Resour. Res.* 42. <https://doi.org/10.1029/2006WR004921>.
- de Louw, P.G.B., Oude Essink, G.H.P., Stuyfzand, P.J., van der Zee, S.E.A.T.M., 2010. Upward groundwater flow in boils as the dominant mechanism of salinization in deep polders, The Netherlands. *J. Hydrol.* 394, 494–506. <https://doi.org/10.1016/j.jhydrol.2010.10.009>.
- Dimova, N.T., Burnett, W.C., Chanton, J.P., Elizabeth, J., 2013. Application of radon-222 to investigate groundwater discharge into small shallow lakes. *J. Hydrol.* 486, 112–122. <https://doi.org/10.1016/j.jhydrol.2013.01.043>.
- Dugdale, S.J., Malcolm, I.A., Kantola, K., Hannah, D.M., 2018. Stream temperature under contrasting riparian forest cover: understanding thermal dynamics and heat exchange processes. *Sci. Total Environ.* 610–611, 1375–1389. <https://doi.org/10.1016/j.scitotenv.2017.08.198>.
- Dujardin, J., Anibas, C., Bronders, J., Jamin, P., Hamonts, K., Dejonghe, W., Brouyère, S., Batelaan, O., 2014. Combining flux estimation techniques to improve characterization of groundwater-surface-water interaction in the Zenne River, Belgium. *Hydrogeol. J.* 1657–1668. <https://doi.org/10.1007/s10040-014-1159-4>.
- Dulaiova, H., Burnett, W.C., 2006. Radon loss across the water-air interface (Gulf of Thailand) estimated, 33, 1–4. <https://doi.org/10.1029/2005GL025023>.
- Eaton, J.G., Scheller, R.M., 1996. Effects of climate warming on fish thermal habitat in streams of the United States. *Limnol. Oceanogr.* 41, 1109–1115. <https://doi.org/10.4319/lo.1996.41.5.1109>.
- Emerson, S., Broecker, W., 1973. Gas-exchange rates in a small lake as determined by the radon method. *J. Fish. Res. Board Canada* 30, 1475–1484.
- Garner, G., Malcolm, I.A., Sadler, J.P., Hannah, D.M., 2017. The role of riparian vegetation density, channel orientation and water velocity in determining river temperature dynamics. *J. Hydrol.* 553, 471–485. <https://doi.org/10.1016/j.jhydrol.2017.03.024>.
- Garner, G., Malcolm, I.A., Sadler, J.P., Hannah, D.M., 2014. What causes cooling water temperature gradients in a forested stream reach? *Hydrol. Earth Syst. Sci.* 18, 5361–5376. <https://doi.org/10.5194/hess-18-5361-2014>.
- Geneux, D.P., Hemond, H.F., 1992. Determination of gas exchange rate constants for a small stream on walker branch watershed, Tennessee. *Water Resour. Res.* 28, 2365–2374.
- Geneux, D.P., Hemond, H.F., 1990. Naturally occurring radon 222 as a tracer for streamflow generation: steady state methodology and field Example. *Water Resour. Res.* 26, 3065–3075. <https://doi.org/10.1029/WR026i012p3065>.
- Gilmore, T.E., Geneux, D.P., Solomon, D.K., Solder, J.E., 2016. Groundwater transit time distribution and mean from streambed sampling in an agricultural coastal plain watershed, North Carolina, USA. *Water Resour. Res.*, 2025–2044. <https://doi.org/10.1002/2015WR017600>.Received.
- Guse, B., Kail, J., Radinger, J., Schröder, M., Kiesel, J., Hering, D., Wolter, C.F., Fohrer, N., 2015. Eco-hydrologic model cascades: Simulating land use and climate change impacts on hydrology, hydraulics and habitats for fish and macroinvertebrates. *Sci. Total Environ.* 533, 542–556. <https://doi.org/10.1016/j.scitotenv.2015.05.078>.
- Haidekker, A., Hering, D., 2008. Relationship between benthic insects (Ephemeroptera, Plecoptera, Coleoptera, Trichoptera) and temperature in small and medium-sized streams in Germany: a multivariate study. *Aquat. Ecol.* 42, 463–481. <https://doi.org/10.1007/s10452-007-9097-z>.
- Hannah, D.M., Malcolm, I.A., Soulsby, C., Youngson, A.F., 2008. A comparison of forest and moorland stream microclimate, heat exchanges and thermal dynamics. *Hydrol. Process.* 22, 919–940. <https://doi.org/10.1002/hyp>.
- Hare, D.K., Briggs, M.A., Rosenberry, D.O., Boutt, D.F., Lane, J.W., 2015. A comparison of thermal infrared to fiber-optic distributed temperature sensing for evaluation of groundwater discharge to surface water. *J. Hydrol.* 530, 153–166. <https://doi.org/10.1016/j.jhydrol.2015.09.059>.
- Harrington, J.S., Hayashi, M., Kurylyk, B.L., 2017. Influence of a rock glacier spring on the stream energy budget and cold-water refuge in an alpine stream. *Hydrol. Process.* 31, 4719–4733. <https://doi.org/10.1002/hyp.11391>.
- Hausner, M.B., Suarez, F., Glander, K.E., Van De Giesen, N.C., Selker, J.S., Tyler, S.W., 2011. Calibrating single-ended fiber-optic raman spectra distributed temperature sensing data. *Sensors* 11, 10859–10879. <https://doi.org/10.3390/s111110859>.
- Hawkins, C.P., Hogue, J.N., Decker, L.M., Feminella, J.W., 1997. Channel Morphology, Water Temperature, and Assemblage Structure of Stream Insects.
- Hayashi, M., Rosenberry, D.O., 2002. Effects of ground water exchange on the hydrology and ecology of surface water. *Ground Water* 40, 309–316.
- Hazelwood, D.H., Hazelwood, S.E., 1985. The effect of temperature on oxygen consumption in four species of freshwater fairy shrimp Crustacea Anostraca. *Freshw. Invertebr. Biol.* 4, 133–137.
- Hilgersom, K.P., Van De Giesen, N.C., de Louw, P.G.B., Zijlema, M., 2016. Three-dimensional dense distributed temperature sensing for measuring layered thermohaline systems. *Water Resour. Res.* 52, 6656–6670. <https://doi.org/10.1029/2008WR006912>.
- Irvine, D.J., Briggs, M.A., Lautz, L.K., Gordon, R.P., McKenzie, J.M., 2017. Using diurnal temperature signals to infer vertical groundwater-surface water exchange. *Ground Water* 55, 10–26. <https://doi.org/10.1111/gwat.12459>.
- Isaak, D.J., Luce, C., Horan, D.L., Chandler, G.L., Wollrab, S.P., Nagel, D.E., 2018. Global warming of salmon and trout Rivers in the Northwestern U.S.: road to ruin or path through purgatory? 566–587. <https://doi.org/10.1002/tafs.10059>.
- Isaak, D.J., Young, M.K., Nagel, D.E., Horan, D.L., Groce, M.C., 2015. The cold-water climate shield: Delineating refugia for preserving salmonid fishes through the 21st century. *Global Change Biol.* 21, 2540–2553. <https://doi.org/10.1111/gcb.12879>.
- Kaandorp, V.P., de Louw, P.G.B., van der Velde, Y., Broers, H.P., 2018a. Transient groundwater travel time distributions and age-ranked storage-discharge relationships of three lowland catchments. *Water Resour. Res.* 1–18. <https://doi.org/10.1029/2017WR022461>.
- Kaandorp, V.P., Molina-Navarro, E., Andersen, H.E., Bloomfield, J.P., Kuijper, M.J.M., de Louw, P.G.B., 2018b. A conceptual model for the analysis of multi-stressors in linked groundwater-surface water systems. *Sci. Total Environ.* 627, 880–895. <https://doi.org/10.1016/j.scitotenv.2018.01.259>.
- Karan, S., Sebok, E., Engesgaard, P., 2017. Air/water/sediment temperature contrasts in small streams to identify groundwater seepage locations. *Hydrol. Process.* 31, 1258–1270. <https://doi.org/10.1002/hyp.11094>.
- Kennedy, C.D., Genereux, D.P., Corbett, D.R., Mitasova, H., 2009. Spatial and temporal dynamics of coupled groundwater and nitrogen fluxes through a streambed in an agricultural watershed. *Water Resour. Res.* 45, 1–18. <https://doi.org/10.1029/2008WR007397>.
- Krause, S., Blume, T., Cassidy, N.J., 2012. Investigating patterns and controls of groundwater up-welling in a lowland river by combining Fibre-optic Distributed Temperature Sensing with observations of vertical hydraulic gradients. *Hydrol. Earth Syst. Sci.* 16, 1775–1792. <https://doi.org/10.5194/hess-16-1775-2012>.
- Kristensen, P.B., Kristensen, E.A., Riis, T., Alnoe, A.B., Larsen, S.E., Vervier, P., Baattrup-Pedersen, A., 2015. Riparian forest as a management tool for moderating future thermal conditions of lowland temperate streams. *Int. Waters* 5, 27–38. <https://doi.org/10.5268/IW-5.1.751>.
- Kurylyk, B.L., MacQuarrie, K.T.B., Caisse, D., McKenzie, J.M., 2015. Shallow groundwater thermal sensitivity to climate change and land cover disturbances: derivation of analytical expressions and implications for stream temperature modeling. *Hydrol. Earth Syst. Sci.* 19, 2469–2489. <https://doi.org/10.5194/hess-19-2469-2015>.
- Kurylyk, B.L., MacQuarrie, K.T.B., Voss, C.I., 2014. Climate change impacts on the temperature and magnitude of groundwater discharge from shallow, unconfined aquifers. *Water Resour. Res.* 50, 3253–3274. <https://doi.org/10.1002/2013WR014588>.
- Kurylyk, B.L., Moore, R.D., MacQuarrie, K.T.B., 2016. Scientific briefing: quantifying streambed heat advection associated with groundwater – surface water interactions. *Hydrol. Process.* 30, 987–992. <https://doi.org/10.1002/hyp.10709>.
- Kurylyk, B.L., Bourque, C.P.-A., MacQuarrie, K.T.B., 2013. Potential surface temperature and shallow groundwater temperature response to climate change: an example from a small forested catchment in east-central NB

- (Canada). *Hydrol. Earth Syst. Sci.* 17, 2701–2716. <https://doi.org/10.5194/hess-17-2701-2013>.
- Kwakman, J.F.M., Versteegh, P.J.M., 2016. Radon-222 in ground water and finished drinking water in the Dutch provinces Overijssel and Limburg. Bilthoven.
- Lowry, C.S., Walker, J.F., Hunt, R.J., Anderson, M.P., 2007. Identifying spatial variability of groundwater discharge in a wetland stream using a distributed temperature sensor. *Water Resour. Res.* 43. <https://doi.org/10.1029/2007WR006145>.
- Macdonald, R.J., Boon, S., Byrne, J.M., Silins, U., 2014. A comparison of surface and subsurface controls on summer temperature in a headwater stream. *Hydrol. Process.* 28, 2338–2347. <https://doi.org/10.1002/hyp.9756>.
- Matheswaran, K., Blemmer, M., Rosbjerg, D., Boegh, E., 2014a. Seasonal variations in groundwater upwelling zones in a Danish lowland stream analyzed using Distributed Temperature Sensing (DTS). *Hydrol. Process.* 28, 1422–1435. <https://doi.org/10.1002/hyp.9690>.
- Matheswaran, K., Blemmer, M., Thorn, P., Rosbjerg, D., Boegh, E., 2014b. Investigation of stream temperature response to non-uniform groundwater discharge in a Danish lowland stream. *River Res. Appl.* <https://doi.org/10.1002/rra.2792>.
- Meisner, J.D., Rosenfeld, J.S., Regier, H.A., 1988. The role of groundwater in the impact of climate warming on stream salmonines. *Fisheries* 13, 2–8. [https://doi.org/10.1577/1548-8446\(1988\)013<0002:TROGIT>2.0.CO;2](https://doi.org/10.1577/1548-8446(1988)013<0002:TROGIT>2.0.CO;2).
- Menberg, K., Blum, P., Kurylyk, B.L., Bayer, P., 2014. Observed groundwater temperature response to recent climate change. *Hydrol. Earth Syst. Sci.* 18, 4453–4466. <https://doi.org/10.5194/hess-18-4453-2014>.
- Monteith, J.L., 1981. Evaporation and surface temperature. *Quart. J. R. Meteorol. Soc.* 107, 1–27.
- Moss, B., Mckee, D., Atkinson, D., Collings, S.E., Eaton, J.W., Gill, A.B., Harvey, I., Hatton, K., Heyes, T., Wilson, D., 2003. How important is climate? Effects of warming, nutrient addition and fish on phytoplankton in shallow lake microcosms. *J. Appl. Ecol.* 40, 782–792. <https://doi.org/10.1046/j.1365-2664.2003.00839.x>.
- Nash, C.S., Selker, J.S., Grant, G.E., Lewis, S.L., Noël, P., 2018. A physical framework for evaluating net effects of wet meadow restoration on late-summer streamflow. *Ecohydrology* 11. <https://doi.org/10.1002/eco.1953>.
- Neilson, B.T., Hatch, C.E., Ban, H., Tyler, S.W., 2010. Solar radiative heating of fiber-optic cables used to monitor temperatures in water. *Water Resour. Res.* 46, 1–17. <https://doi.org/10.1029/2009WR008354>.
- Null, S.E., Viers, J.H., Deas, M.L., Tanaka, S.K., Mount, J.F., 2012. Stream temperature sensitivity to climate warming in California's Sierra Nevada: impacts to coldwater habitat. *Clim. Change* 116, 149–170. <https://doi.org/10.1007/s10584-012-0459-8>.
- Ormerod, S.J., 2009. Climate change, river conservation and the adaptation challenge. *Aquat. Conserv. Mar. Freshwater Ecosyst.* 613, 609–613. <https://doi.org/10.1002/aqc>.
- Piggott, J.J., Townsend, C.R., Matthaei, C.D., 2015. Climate warming and agricultural stressors interact to determine stream macroinvertebrate community dynamics. *Global Change Biol.* 21, 1887–1906. <https://doi.org/10.1111/gcb.12861>.
- Poole, G.C., Berman, C.H., 2001. An ecological perspective on in-stream temperature: natural heat dynamics and mechanisms of human-caused thermal degradation. *Environ. Manage.* 27, 787–802. <https://doi.org/10.1007/s002670010188>.
- Poulsen, J.R., Sebok, E., Duque, C., Tetzlaff, D., Engesgaard, P.K., 2015. Detecting groundwater discharge dynamics from point-to-catchment scale in a lowland stream: combining hydraulic and tracer methods. *Hydrol. Earth Syst. Sci.* 19, 1871–1886. <https://doi.org/10.5194/hess-19-1871-2015>.
- Power, G., Brown, R.S., Imhof, J.G., 1999. Groundwater and fish – insights from northern North America. *Hydrol. Process.* 422, 401–422.
- Rasmussen, J.J., Baattrup-Pedersen, A., Riis, T., Friberg, N., 2011. Stream ecosystem properties and processes along a temperature gradient. *Aquat. Ecol.* 45, 231–242. <https://doi.org/10.1007/s10452-010-9349-1>.
- Rau, G.C., Andersen, M.S., Acworth, R.I., 2012. Experimental investigation of the thermal dispersivity term and its significance in the heat transport equation for flow in sediments. *Water Resour. Res.* 48, 1–21. <https://doi.org/10.1029/2011WR011038>.
- Rosenberry, D.O., Briggs, M.A., Delin, G., Hare, D.K., 2016. Combined use of thermal methods and seepage meters to efficiently locate, quantify, and monitor focused groundwater discharge to a sand-bed stream. *Water Resour. Res.* 52, 4486–4503. <https://doi.org/10.1002/2016WR018808>.
- Schülting, L., Feld, C.K., Graf, W., 2016. Effects of hydro- and thermopeaking on benthic macroinvertebrate drift. *Sci. Total Environ.* <https://doi.org/10.1016/j.scitotenv.2016.08.022>.
- Sebok, E., Duque, C., Engesgaard, P., Boegh, E., 2015. Application of distributed temperature sensing for coupled mapping of sedimentation processes and spatio-temporal variability of groundwater discharge in soft-bedded streams. *Hydrol. Process.* 29, 3408–3422. <https://doi.org/10.1002/hyp.10455>.
- Sebok, E., Duque, C., Kazmierczak, J., Engesgaard, P.K., Nilsson, B., Karan, S., Frandsen, M., 2013. High-resolution distributed temperature sensing to detect seasonal groundwater discharge into Lake Vaeng, Denmark. *Water Resour. Res.* 49, 5355–5368. <https://doi.org/10.1002/wrcr.20436>.
- Selker, J.S., Thévenaz, L., Huwald, H., Mallet, A., Luxemburg, W., Van De Giesen, N.C., Stejskal, M., Zeman, J., Westhoff, M.C., Parlange, M.B., 2006. Distributed fiber-optic temperature sensing for hydrologic systems. *Water Resour. Res.* 42, 1–8. <https://doi.org/10.1029/2006WR005326>.
- Sweeney, B.W., Newbold, J.D., 2014. Streamside forest buffer width needed to protect stream water quality, habitat, and organisms: a literature review. *J. Am. Water Resour. Assoc.* 50, 560–584. <https://doi.org/10.1111/jawr.12203>.
- Taylor, C.A., Stefan, H.G., 2009. Shallow groundwater temperature response to climate change and urbanization. *J. Hydrol.* 375, 601–612. <https://doi.org/10.1016/j.jhydrol.2009.07.009>.
- Thomas, S.M., Griffiths, S.W., Ormerod, S.J., 2015. Adapting streams for climate change using riparian broadleaf trees and its consequences for stream salmonids. *Freshw. Biol.* 60, 64–77. <https://doi.org/10.1111/fwb.12467>.
- Van De Giesen, N.C., Steele-Dunne, S.C., Jansen, J., Hoes, O., Hausner, M.B., Tyler, S.W., Selker, J.S., 2012. Double-ended calibration of fiber-optic raman spectra distributed temperature sensing data. *Sensors (Switzerland)* 12, 5471–5485. <https://doi.org/10.3390/s120505471>.
- van den Hoek, T.H., Verdonschot, P.F.M., 2001. De invloed van veranderingen in temperatuur op beek- macrofauna. Wageningen.
- van der Aa, N.G.F.M., Goes, B.J.M., de Louw, P.G.B., den Otter, C., Reckman, J.W.T.M., Stuurman, R.J., 1999. Ecohydrologische Systemanalyse. Springendalse Beek, Delft.
- van Ommen, H.C., 1986. Influence of diffuse sources of contamination on the quality of outflowing groundwater including non-equilibrium adsorption and decomposition. *J. Hydrol.* 88, 79–95.
- Van Vliet, M.T.H., Franssen, W.H.P., Yearsley, J.R., Ludwig, F., Haddeland, I., Lettenmaier, D.P., Kabat, P., 2013. Global river discharge and water temperature under climate change. *Glob. Environ. Chang.* 23, 450–464. <https://doi.org/10.1016/j.gloenvcha.2012.11.002>.
- van Walsum, P.E.V., Verdonschot, P.F.M., Runhaar, J., 2002. Effects of climate and land-use change on lowland stream ecosystems. Wageningen.
- Vandenbohede, A., de Louw, P.G.B., Doornenbal, P.J., 2014. Characterizing preferential groundwater discharge through boils using temperature. *J. Hydrol.* 510, 372–384. <https://doi.org/10.1016/j.jhydrol.2014.01.006>.
- Vannote, R.L., Sweeney, B.W., 1980. Geographic analysis of thermal equilibria: a conceptual model for evaluating the effect of natural and modified thermal regimes on aquatic insect communities 115, 667–695.
- Verdonschot, P.F.M., 1990. Ecological characterization of surface waters in the province of Overijssel, The Netherlands. Thesis 255.
- Wallin, M.B., Öquist, M.G., Buffam, I., Billett, M.F., Nisell, J., Bishop, K.H., 2011. Spatiotemporal variability of the gas transfer coefficient (K<sub>CO2</sub>) in boreal streams: Implications for large scale estimates of CO<sub>2</sub> evasion. *Glob. Biogeochem. Cycles* 25, 1–14. <https://doi.org/10.1029/2010GB003975>.
- Ward, J. V., Stanford, J.A., 1982. Evolutionary Ecology of Aquatic Insects, 97–117.
- Watts, G., Battarbee, R.W., Bloomfield, J.P., Crossman, J., Daccache, A., Durance, I., Elliott, J.A., Garner, G., Hannaford, J., Hannah, D.M., Hess, T., Jackson, C.R., Kay, A. L., Kernan, M., Knox, J., Mackay, J., Monteith, D.T., Ormerod, S.J., Rance, J., Stuart, M.E., Wade, A.J., Wade, S.D., Weatherhead, K., Whitehead, P.G., Wilby, R.L., 2015. Climate change and water in the UK – past changes and future prospects. *Prog. Phys. Geogr.* 39, 6–28. <https://doi.org/10.1177/0309133314542957>.
- Webb, B.W., Nobilis, F., 2007. Long-term changes in river temperature and the influence of climatic and hydrological factors. *Hydrol. Sci. J.* 52, 74–85. <https://doi.org/10.1623/hysj.52.1.74>.
- Westhoff, M.C., Bogaard, T.A., Savenije, H.H.G., 2011. Quantifying spatial and temporal discharge dynamics of an event in a first order stream, using distributed temperature sensing. *Hydrol. Earth Syst. Sci.* 15, 1945–1957. <https://doi.org/10.5194/hess-15-1945-2011>.
- Westhoff, M.C., Savenije, H.H.G., Luxemburg, W.M.J., Stelling, G.S., Van De, N.C., Selker, J.S., Pfister, L., Uhlenbrook, S., 2007. A distributed stream temperature model using high resolution temperature observations. *Hydrol. Earth Syst. Sci.* 11, 1469–1480.
- Yu, L., Rozemeijer, J.C., van der Velde, Y., van Breukelen, B.M., Ouboter, M., Broers, H. P., 2019. Urban hydrogeology: transport routes and mixing of water and solutes in a groundwater influenced urban lowland catchment. Manuscript submitted for publication.
- Ylla, I., Canhoto, C., Romaní, A.M., 2014. Effects of warming on stream biofilm organic matter use capabilities. *Microb. Ecol.* 68, 132–145. <https://doi.org/10.1007/s00248-014-0406-5>.
- Zappa, C.J., Raymond, P.A., Terray, E.A., McGillis, W.R., 2003. Variation in surface turbulence and the gas transfer velocity over a tidal cycle in a macro-tidal estuary. *Estuaries* 26, 1401–1415.